Postprint of: Dastjerdi S., Akgöz B., Civalek Ö., Malikan M., Eremeyev VA. On the non-linear dynamics of torus-shaped and cylindrical shell structures. INTERNATIONAL JOURNAL OF ENGINEERING SCIENCE Vol. 156 (2020), 103371 DOI: 10.1016/j.ijengsci.2020.103371

On the non-linear dynamics of torus-shaped and cylindrical shell structures

Shahriar Dastjerdi [a, b], Bekir Akgöz [b], Ömer Civalek [c], Mohammad Malikan [d], Victor A. Eremeyev [d, e*]

[a] Department of Mechanical Engineering, Shahrood Branch, Islamic Azad University, Shahrood, Iran

[b] Division of Mechanics, Civil Engineering Department, Akdeniz University, Antalya, Turkey

[c] China Medical University, Taichung, Taiwan

[d] Department of Mechanics of Materials and Structures, Faculty of Civil and Environmental Engineering, Gdansk University of Technology, Gdansk, Poland

[e] R. E. Alekseev Nizhny Novgorod Technical University, Minin St., 24, Nizhny Novgorod, 603950 Russia

* Corresponding author: victor.eremeev@pg.edu.pl, eremeyev.victor@gmail.com

ABSTRACT

In this study, the non-linear dynamic analysis of torus-shaped and cylindrical shell-like structures has been studied. The applied material is assumed as the functionally graded material (FGM). The structures are considered to be used for important machines such as wind turbines. The effects of some environmental factors on the analysis like temperature and humidity have been considered. The strain field has been calculated in general form and in continue the dynamic governing equations of torus structure have been derived based on the first-order shear deformation theory. The rotation around two independent axes in the torus coordinate system is considered and time-dependent equations are solved using SAPM semi-analytical method. The stresses and deformations generated in the torus and cylindrical shaped structures are plotted. The rotation of structures has been attended due to some transportation purposes. The

effect of internal pressures as well as rotational speed at torus and cylindrical structures has been investigated in several numerical diagrams. The results are presented in the form of graphs that consider the rotational effects, loading, thermal and humid (hygro-thermal) environments, and size of the structures. This research can provide scientific perspectives to researchers who will examine the dynamic analysis of torus and cylindrical shaped structures.

Keywords: Torus-shape and cylindrical structures; Dynamic analysis; Functionally graded materials; First-order shear deformation theory (FSDT); hygro-thermal environment

1. Introduction

Torus geometry can be dedicated as the most basic dynamical geometries [1-3]. On the importance of the torus geometry, it can be stated that some scientists have proposed the theory of torus-shaped universe. This means the universe may be formed in a three-dimensional torus geometry [4, 5].

One of the significant engineering applications of the torus and cylindrical shell-like structures can be found in the wind turbines [6, 7]. There are criticizes with offshore wind turbines due to their low efficiency in absorbing and delivering the wind energy. Another shortcoming of these machines is that some energy produced from the machine is often lost. To improve the efficiency of the wind turbines and utilize fully the ocean wind energy and reduce the costs, a torus frame and or a cylindrical shape have been contemplating by designer engineers for recent years. A torus-shaped wave energy converter, which is called spar-torus combination (STC) wind turbine, is one of the best dynamical machines. The designation of the new machines resulted in the high storage of the generated energy in the both kinetic and efficient frameworks. A torus structure can create high kinetic energy. The machine's structure includes a combination of a hollow torus ring beside some shell-like parts and a vertical wind turbine which leads to a massive flywheel. Within the design of the wind turbines, the focal

point can be the structural section involving re-entry cold and hot structures, structural dynamics and stable and lightweight structures. To deal with this, the novel techniques have come to give the best tools for mechanical analysis in experiment. There are active and passive noise, vibrations, variations of temperature, humidity, impacts of internal pressures and the other passive mechanical loads that a wind turbine configuration confronts with them [8-21].

In a wind turbine machine, moisture generally arises within the parts. As the sea's humidity variations are unavoidable, then establishing harmful effects of moisture can be expressed as a serious discussion for wind turbines [22]. In fact, it would be transferred to the structures of the machine and consequently damage it. It is so significant to predict this humidity in structural design of the new wind turbines. This way, the machine and equipment would all stand safe. The prediction of moisture's influence in the structural behavior of a wind turbine helps to avoid its problems. If the moisture percentage goes higher, there will be difficulties for not only life cycle of the parts of the machine but also its efficiency. The higher the moisture percentage, the lower the density of air. Then, a lower output power from turbine will be implied by condensed air [23]. High percentage of the moisture would lead to internal pressure of the machine by condensation process of the air, as well. Thus, it is crucial to pre-analysis the humidity on the structures of a wind turbine consisting of the torus structure.

From the point of view of the mechanism of work, sea is completely serious with what we have on the ground, and different stochastic conditions govern it. During working of a turbine in the sea, components and parts of the machine that are working in contact together will heat up. The conditions are more serious when the machine has to be working continuously without any rest. Therefore, the parts of the machine are subjected to the temperature hazards and the life cycle of the parts would be affected remarkably. Thus, working in this thermal environment can harm the flexible structures of the wind turbine, and it can be stated that the

machine is susceptible to be seriously damaged. Not only the temperature would affect the life cycle of the machine's parts, but also the high temperature can affect the output energy. The density of air is low when the temperature is high, hence, the output energy will be lessened. Contrariwise, when the temperature is too low, it may freeze the parts and the machine will be stopped [24, 25]. Moreover, as the dynamic working of this machine is time-dependent based on the changes in rotational movement due to the variations in the wind speed, it would be more critical in combination with temperature. Therefore, temperature-time dependent coupling dynamic analysis is an earnestly request addressed in this paper.

The increasing requires having better knowledge on the structural dynamics of fundamental geometries. This research paper performs a theoretical and computational dynamic modelling of torus and shell-like structures. In doing so, functionally graded materials (FGMs) [26-34] are developed to be modelled as torus and cylindrical structures. Mathematical modelling and obtaining time-dependent relations are based on the first-order shear deformation theory. In order to further identify the structural dynamic response of these geometries, temperature variations and humidity are taken into the investigation. It was tried to attain a general media on the dynamics of the torus parts on the basis of general strain field so that it can be converted and transferred into different strain fields. Simulations are regarding SAPM semi-analytical solution technique [34-36]. Pictorial diagrams based on stress analysis are evaluated for two mentioned geometries, that are torus and cylindrical shapes. Another intention is to demonstrate optimized outcomes for some critical factors and define the allowable tolerances. As results of several cases, it is expected that internal pressures in the torus geometry affect notably its structure. For this aim, the performance of both torus and cylindrical chambers are estimated exposed to internal pressures. More importantly, rotational speed is considered for both aforesaid shapes, of course, for the torus one it is based on the two independent axes.

In the end, different illustrations based on numerical results are prepared to reveal effects of all key cases.

In continuation, the paper is organized as follows: section 2 helps us to know a bit about STC wind turbines. In section 3, and 4, we model mathematically the torus-shaped and cylindrical-shaped structures. By means of section 5, the analysis of dynamic stresses is shown. Moreover, section 6 will present a validity for results and demonstrate numerical outcomes. In addition to these, section 7 will finalize the paper by illustrating a brief conclusion and vital results.

2. A floating STC wind turbine

As seen by Fig. 1, a STC wind turbine is demonstrated (the picture is not scaled correctly). The different sections are named in the picture. The torus part can be replaced by a cylindrical one. In this paper, we also compare dynamically these two shapes to each other. The torus is exactly placed on the sea surface and is rotated by the aid of water waves. Generally, in STC the blades convert the wind energy and the torus (or cylinder) converts the water waves energy into the electricity energy.

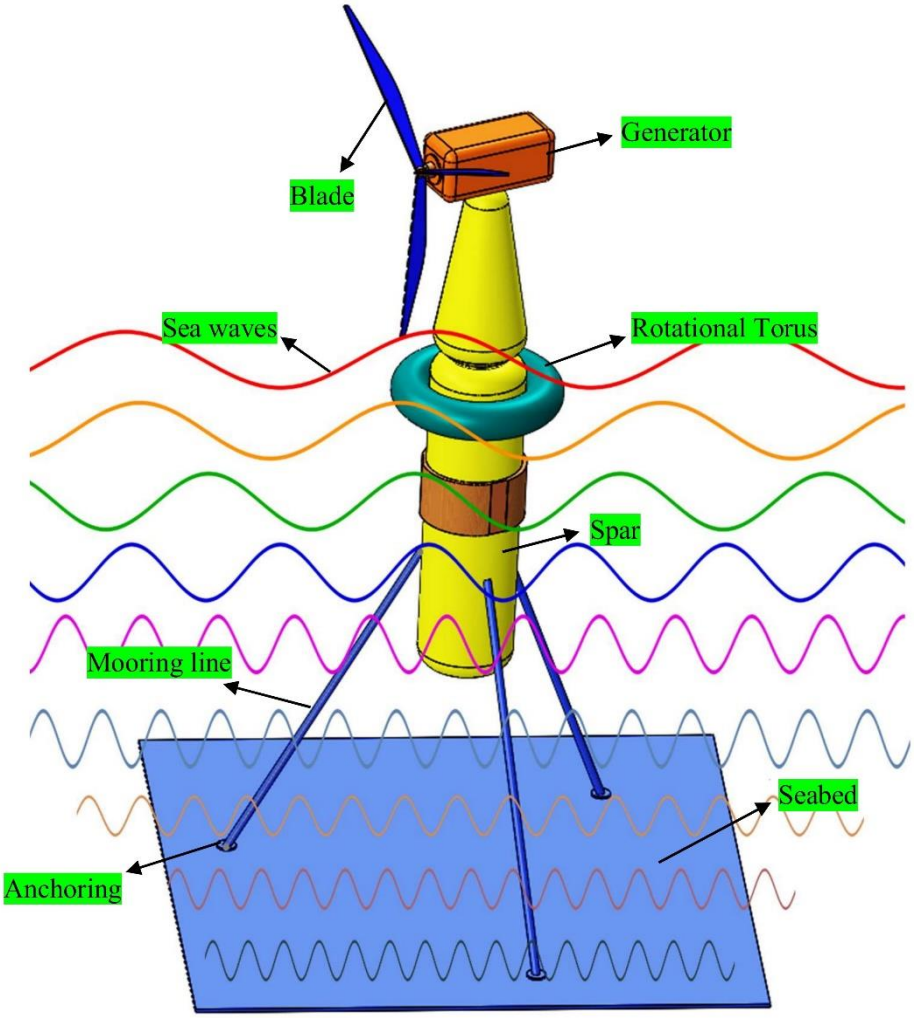

Fig. 1. The schematic view of a STC wind turbine

3. Dynamic analysis of a torus-shaped structure

In this section, the governing equations of a ring torus shell will be derived. This structure can be part of a complete torus structure along θ and α directions. Therefore, there are no restrictions and a wide range of geometric shapes of torus shapes can be examined. According to Fig. 2, the changes will be in both θ and α directions. θ and α angles can vary from 0 to 2 □. If both θ and α are selected as 2 □, a complete donut structure will be made (Fig. 3). If the smaller radius r is considered constantly, then $r = R$. The bigger radius of the ring torus is assumed R_t (Fig. 2). It is important to note that the cylindrical structure can also be simulated

by selecting the torus radius (R_t) and the angles α_1 and α_1 according to calculations as follows which will eventually obtain the cylindrical geometric [37, 38] shape based on the donut-shaped structure.

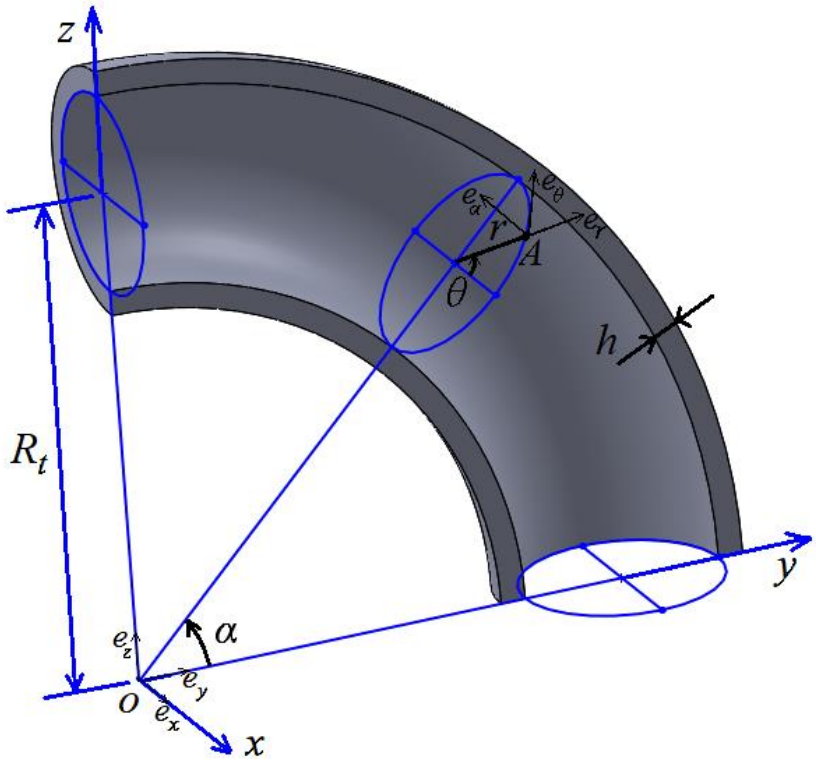

Fig. 2. The schematic view of an angular torus structure in Toroidal and Cartesian Coordinate systems

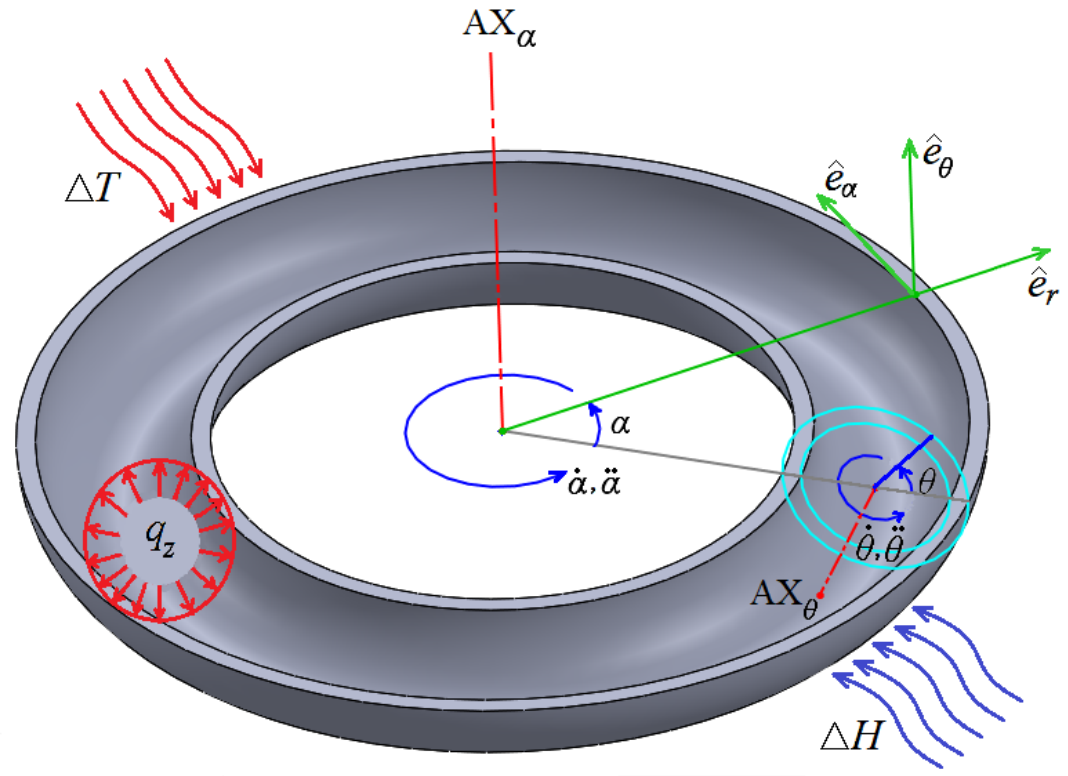

Fig. 3. The complete ring torus structure rotating around two axes of AX_α and AX_θ under internal pressure and hygro-thermal environment

$$R_t = \infty; L = R_t\left(\alpha_2 - \alpha_1\right); R_1 = R \qquad L \text{ is the length of cylinder} \tag{1}$$

Therefore, according to the explanations provided, the analysis of the donut-shaped structure is more general and with the accordance simulation, the cylindrical structure can also be examined.

The variables change in the considered coordinate system in Fig. 2 (torus coordinate system) will be in the three directions r, θ and α.

According to Fig. 2, the relationship between the Cartesian coordinate system and the Torus coordinate system will be as follows:

$$
\begin{cases} x = r\cos(\theta) \\ y = (R_t + r\sin(\theta))\cos(\alpha) \\ z = (R_t + r\sin(\theta))\sin(\alpha) \end{cases}
$$

$$
\Rightarrow \begin{cases} \dfrac{\partial}{\partial x} = \dfrac{\partial}{\partial r}(\cos(\theta)) + \dfrac{\partial}{\partial \theta}(-r\sin(\theta)) \\ \dfrac{\partial}{\partial y} = \dfrac{\partial}{\partial r}(\sin(\theta)\cos(\alpha)) + \dfrac{\partial}{\partial \theta}(r\cos(\theta)\cos(\alpha)) + \dfrac{\partial}{\partial \alpha}(-\sin(\alpha)(R_t + r\sin(\theta))) \\ \dfrac{\partial}{\partial z} = \dfrac{\partial}{\partial r}(\sin(\theta)\sin(\alpha)) + \dfrac{\partial}{\partial \theta}(r\cos(\theta)\sin(\alpha)) + \dfrac{\partial}{\partial \alpha}(\cos(\alpha)(R_t + r\sin(\theta))) \end{cases}
$$

$$
\Rightarrow \begin{cases} \dfrac{\partial}{\partial r} = \dfrac{\partial}{\partial x}(\cos(\theta)) + \dfrac{\partial}{\partial y}(\sin(\theta)\cos(\alpha)) + \dfrac{\partial}{\partial z}(\sin(\theta)\sin(\alpha)) \\ \dfrac{\partial}{\partial \theta} = \dfrac{\partial}{\partial x}\left(-\dfrac{1}{r}\sin(\theta)\right) + \dfrac{\partial}{\partial y}\left(\dfrac{1}{r}\cos(\theta)\cos(\alpha)\right) + \dfrac{\partial}{\partial z}\left(\dfrac{1}{r}\cos(\theta)\sin(\alpha)\right) \\ \dfrac{\partial}{\partial \alpha} = \dfrac{\partial}{\partial y}\left(\dfrac{-\sin(\alpha)}{(R_t + r\sin(\theta))}\right) + \dfrac{\partial}{\partial z}\left(\dfrac{\cos(\alpha)}{(R_t + r\sin(\theta))}\right) \end{cases} \tag{2}
$$

As a result, according to the above calculations, it can be concluded that the gradient of change (∇) is:

$$
\nabla = \begin{bmatrix} \dfrac{\partial}{\partial r} & \dfrac{1}{r}\dfrac{\partial}{\partial \theta} & \dfrac{1}{(R_t + r\sin(\alpha))}\dfrac{\partial}{\partial \alpha} \end{bmatrix} \tag{3}
$$

The relationships between the unit vectors in the Cartesian coordinate system and the Torus coordinate system will be obtained as follows:

$$
\begin{cases} e_r = e_x(\cos(\theta)) + e_y(\sin(\theta)\cos(\alpha)) + e_z(\sin(\theta)\sin(\alpha)) \\ e_\theta = e_x(-\sin(\theta)) + e_y(\cos(\theta)\cos(\alpha)) + e_z(\cos(\theta)\sin(\alpha)) \\ e_\alpha = e_y(-\sin(\alpha)) + e_z(\cos(\alpha)) \end{cases} \tag{4}
$$

Also, the changes in the unit vectors e_r , e_θ and e_α in the three main directions *r*, θ, and α are written as the following relations:

$$\begin{bmatrix} \frac{\partial e_r}{\partial r}=0 & \frac{\partial e_r}{\partial \theta}=e_\theta & \frac{\partial e_r}{\partial \alpha}=\left(\sin(\theta)\right)e_\alpha \\ \frac{\partial e_\theta}{\partial r}=0 & \frac{\partial e_\theta}{\partial \theta}=-e_r & \frac{\partial e_\theta}{\partial \alpha}=\left(\cos(\theta)\right)e_\alpha \\ \frac{\partial e_\alpha}{\partial r}=0 & \frac{\partial e_\alpha}{\partial \theta}=0 & \frac{\partial e_\alpha}{\partial \alpha}=\left(-\sin(\theta)\right)e_r+\left(-\cos(\theta)\right)e_\theta \end{bmatrix} \tag{5}$$

The following tensor equation can be used to obtain the strain tensor in the Torus coordinate system (Fig. 2).

$$\varepsilon=\frac{1}{2}\left[\nabla U+\nabla U^T+\nabla U\cdot\nabla U^T\right] \tag{6}$$

In the above equation, the gradient operator (∇) changes according to Eq. (3). Also, U is the displacement field, which according to the coordinate system mentioned in the three directions of r, θ and α is presented according to the following vector.

$$U=\left[U_r e_r \quad U_\theta e_\theta \quad U_\alpha e_\alpha\right] \tag{7}$$

It can be possible to obtain ∇U and then ∇U^T now. A non-linear term is also observed in Eq. 7 as $\nabla U\cdot\nabla U^T$.

$$\nabla U=\begin{bmatrix} \frac{\partial}{\partial r}\left(e_r\right) & \frac{1}{r}\frac{\partial}{\partial \theta}\left(e_\theta\right) & \frac{1}{\left(R_t+r\sin(\alpha)\right)}\frac{\partial}{\partial \alpha}\left(e_\alpha\right) \end{bmatrix}\begin{bmatrix} U_r\left(e_r\right) \\ U_\theta\left(e_\theta\right) \\ U_\alpha\left(e_\alpha\right) \end{bmatrix} \tag{8}$$

Therefore, each of the 9 elements in the strain tensor can be calculated and written in a 3×3 matrix below.

$$\nabla U=\begin{bmatrix} U_{rr} & U_{r\theta} & U_{r\alpha} \\ U_{\theta r} & U_{\theta\theta} & U_{\theta\alpha} \\ U_{\alpha r} & U_{\alpha\theta} & U_{\alpha\alpha} \end{bmatrix} \tag{9}$$

Now expanding Eq. (8) (and considering the derivatives in Eq. (5)) can lead to the following equations.

$$
\begin{cases}
\left(e_r\right)\dfrac{\partial}{\partial r}\left[U_r\left(e_r\right)\right]=e_r e_r\dfrac{\partial U_r}{\partial r}+e_r U_r\dfrac{\partial e_r}{\partial r}=e_r e_r\dfrac{\partial U_r}{\partial r}\\
\left(e_r\right)\dfrac{\partial}{\partial r}\left[U_\theta\left(e_\theta\right)\right]=e_r e_\theta\dfrac{\partial U_\theta}{\partial r}+e_r U_\theta\dfrac{\partial e_\theta}{\partial r}=e_r e_\theta\dfrac{\partial U_\theta}{\partial r}\\
\left(e_r\right)\dfrac{\partial}{\partial r}\left[U_\alpha\left(e_\alpha\right)\right]=e_r e_\alpha\dfrac{\partial U_\alpha}{\partial r}+e_r U_\alpha\dfrac{\partial e_\alpha}{\partial r}=e_r e_\alpha\dfrac{\partial U_\alpha}{\partial r}
\end{cases}
$$

$$
\begin{cases}
\left(e_\theta\right)\dfrac{1}{r}\dfrac{\partial}{\partial\theta}\left[U_r\left(e_r\right)\right]=e_\theta e_r\dfrac{1}{r}\dfrac{\partial U_r}{\partial\theta}+e_\theta\dfrac{1}{r}U_r\dfrac{\partial e_r}{\partial\theta}=e_\theta e_r\dfrac{1}{r}\dfrac{\partial U_r}{\partial\theta}+e_\theta e_\theta\dfrac{U_r}{r}\\
\left(e_\theta\right)\dfrac{1}{r}\dfrac{\partial}{\partial\theta}\left[U_\theta\left(e_\theta\right)\right]=e_\theta e_\theta\dfrac{1}{r}\dfrac{\partial U_\theta}{\partial\theta}+e_\theta\dfrac{1}{r}U_\theta\dfrac{\partial e_\theta}{\partial\theta}=e_\theta e_\theta\dfrac{1}{r}\dfrac{\partial U_\theta}{\partial\theta}+e_\theta e_r\left(-\dfrac{U_\theta}{r}\right)\\
\left(e_\theta\right)\dfrac{1}{r}\dfrac{\partial}{\partial\theta}\left[U_\alpha\left(e_\alpha\right)\right]=e_\theta e_\alpha\dfrac{1}{r}\dfrac{\partial U_\alpha}{\partial\theta}+e_\theta\dfrac{1}{r}U_\alpha\dfrac{\partial e_\alpha}{\partial\theta}=e_\theta e_\alpha\dfrac{1}{r}\dfrac{\partial U_\alpha}{\partial\theta}
\end{cases}
$$

$$
\begin{cases}
\left(e_\alpha\right)\dfrac{1}{\left(R_t+r\sin\left(\theta\right)\right)}\dfrac{\partial}{\partial\alpha}\left[U_r\left(e_r\right)\right]=e_\alpha e_r\dfrac{1}{\left(R_t+r\sin\left(\theta\right)\right)}\dfrac{\partial U_r}{\partial\alpha}+e_\alpha\dfrac{1}{\left(R_t+r\sin\left(\theta\right)\right)}U_r\dfrac{\partial e_r}{\partial\alpha}\\
=e_\alpha e_r\dfrac{1}{\left(R_t+r\sin\left(\theta\right)\right)}\dfrac{\partial U_r}{\partial\alpha}+e_\alpha e_\alpha\left(\dfrac{U_r\sin\left(\theta\right)}{\left(R_t+r\sin\left(\theta\right)\right)}\right)\\
\left(e_\alpha\right)\dfrac{1}{\left(R_t+r\sin\left(\theta\right)\right)}\dfrac{\partial}{\partial\alpha}\left[U_\theta\left(e_\theta\right)\right]=e_\alpha e_\theta\dfrac{1}{\left(R_t+r\sin\left(\theta\right)\right)}\dfrac{\partial U_\theta}{\partial\alpha}+e_\alpha\dfrac{1}{\left(R_t+r\sin\left(\theta\right)\right)}U_\theta\dfrac{\partial e_\theta}{\partial\alpha}\\
=e_\alpha e_\theta\dfrac{1}{\left(R_t+r\sin\left(\theta\right)\right)}\dfrac{\partial U_\theta}{\partial\alpha}+e_\alpha e_\alpha\left(\dfrac{U_\theta\cos\left(\theta\right)}{\left(R_t+r\sin\left(\theta\right)\right)}\right)\\
\left(e_\alpha\right)\dfrac{1}{\left(R_t+r\sin\left(\theta\right)\right)}\dfrac{\partial}{\partial\alpha}\left[U_\alpha\left(e_\alpha\right)\right]=e_\alpha e_\alpha\dfrac{1}{\left(R_t+r\sin\left(\theta\right)\right)}\dfrac{\partial U_\alpha}{\partial\alpha}+e_\alpha\dfrac{1}{\left(R_t+r\sin\left(\theta\right)\right)}U_\alpha\dfrac{\partial e_\alpha}{\partial\alpha}\\
=e_\alpha e_\alpha\dfrac{1}{\left(R_t+r\sin\left(\theta\right)\right)}\dfrac{\partial U_\alpha}{\partial\alpha}+e_\alpha e_\theta\left(-\dfrac{U_\alpha\cos\left(\theta\right)}{\left(R_t+r\sin\left(\theta\right)\right)}\right)+e_\alpha e_r\left(-\dfrac{U_\alpha\sin\left(\theta\right)}{\left(R_t+r\sin\left(\theta\right)\right)}\right)
\end{cases}
\tag{10}
$$

Each of elements in Eq. (9) can be obtained by adding similar values in Eq. (10) and rewriting Eq. (9) according to the 3×3 matrix in below.

$$\nabla U = \begin{bmatrix} \frac{\partial U_r}{\partial r} & \frac{\partial U_\theta}{\partial r} & \frac{\partial U_\alpha}{\partial r} \\ \frac{1}{r}\left(\frac{\partial U_r}{\partial \theta} - U_\theta\right) & \frac{1}{r}\left(\frac{\partial U_\theta}{\partial \theta} + U_r\right) & \frac{1}{r}\frac{\partial U_\alpha}{\partial \theta} \\ \frac{1}{\left(R_t + r\sin(\theta)\right)} & \frac{1}{\left(R_t + r\sin(\theta)\right)} & \frac{1}{\left(R_t + r\sin(\theta)\right)} \\ \left(\frac{\partial U_r}{\partial \alpha} - U_\alpha \sin(\theta)\right) & \left(\frac{\partial U_\theta}{\partial \alpha} - U_\alpha \cos(\theta)\right) & \left(U_r \sin(\theta) + U_\theta \cos(\theta) + \frac{\partial U_\alpha}{\partial \alpha}\right) \end{bmatrix} \tag{11}$$

Now ∇U^T can be obtained as the following matrix according to Matrix 11.

$$\nabla U^T = \begin{bmatrix} \frac{\partial U_r}{\partial r} & \frac{1}{r}\left(\frac{\partial U_r}{\partial \theta} - U_\theta\right) & \frac{1}{\left(R_t + r\sin(\theta)\right)}\left(\frac{\partial U_r}{\partial \alpha} - U_\alpha \sin(\theta)\right) \\ \frac{\partial U_\theta}{\partial r} & \frac{1}{r}\left(\frac{\partial U_\theta}{\partial \theta} + U_r\right) & \frac{1}{\left(R_t + r\sin(\theta)\right)}\left(\frac{\partial U_\theta}{\partial \alpha} - U_\alpha \cos(\theta)\right) \\ \frac{\partial U_\alpha}{\partial r} & \frac{1}{r}\frac{\partial U_\alpha}{\partial \theta} & \frac{1}{\left(R_t + r\sin(\theta)\right)}\left(U_r \sin(\theta) + U_\theta \cos(\theta) + \frac{\partial U_\alpha}{\partial \alpha}\right) \end{bmatrix} \tag{12}$$

According to the obtained matrices (matrices 11 and 12) and substituting into Eq. (6), the non-linear strain tensor can be obtained according to the following final matrix whose elements are written separately. It is noted that α_T and β are the thermal expansion and moisture coefficients. Also, $\Delta T = (T_2 - T_1)$ and $\Delta H = (H_2 - H_1)$ are the temperature and moisture percentage differences. Combination of thermal and moisture is defined as hygro-thermal environment. Consequently, the total strain tensor is equal to summation of mechanical (generated by loading) and hygro-thermal (generated by temperature difference and humid environment) strains according to the superposition principle.

$$\varepsilon_{ij}=\begin{bmatrix}\varepsilon_{rr} & \varepsilon_{r\theta} & \varepsilon_{r\alpha}\\ \varepsilon_{\theta r} & \varepsilon_{\theta\theta} & \varepsilon_{\theta\alpha}\\ \varepsilon_{\alpha r} & \varepsilon_{\alpha\theta} & \varepsilon_{\alpha\alpha}\end{bmatrix}-\left(\alpha_T\Delta T+\beta\Delta H\right)\begin{bmatrix}1 & 0 & 0\\ 0 & 1 & 0\\ 0 & 0 & 1\end{bmatrix}$$

$$\varepsilon_{rr}=\left(\frac{\partial U_r}{\partial r}\right)+\frac{1}{2}\left(\left(\frac{\partial U_r}{\partial r}\right)^2+\left(\frac{\partial U_\theta}{\partial r}\right)^2+\left(\frac{\partial U_\alpha}{\partial r}\right)^2\right)$$

$$2\varepsilon_{r\theta}=2\varepsilon_{\theta r}=\frac{1}{r}\left(\frac{\partial U_r}{\partial\theta}-U_\theta\right)+\left(\frac{\partial U_\theta}{\partial r}\right)+\frac{1}{r}\left(\left(\frac{\partial U_r}{\partial r}\right)\left(\frac{\partial U_r}{\partial\theta}-U_\theta\right)+\left(\frac{\partial U_\theta}{\partial r}\right)\left(\frac{\partial U_\theta}{\partial\theta}+U_r\right)+\left(\frac{\partial U_\alpha}{\partial r}\right)\left(\frac{\partial U_\alpha}{\partial\theta}\right)\right)$$

$$2\varepsilon_{r\alpha}=2\varepsilon_{\alpha r}=\frac{1}{\left(R_t+r\sin(\theta)\right)}\left(\frac{\partial U_r}{\partial\alpha}-U_\alpha\sin(\theta)\right)+\left(\frac{\partial U_\alpha}{\partial r}\right)+\frac{1}{\left(R_t+r\sin(\theta)\right)}\left(\left(\frac{\partial U_r}{\partial r}\right)\left(\frac{\partial U_r}{\partial\alpha}-U_\alpha\sin(\theta)\right)+\left(\frac{\partial U_\theta}{\partial r}\right)\left(\frac{\partial U_\theta}{\partial\alpha}-U_\alpha\cos(\theta)\right)+\left(\frac{\partial U_\alpha}{\partial r}\right)\left(U_r\sin(\theta)+U_\theta\cos(\theta)+\frac{\partial U_\alpha}{\partial\alpha}\right)\right)$$

$$\varepsilon_{\theta\theta}=\frac{1}{r}\left(\frac{\partial U_\theta}{\partial\theta}+U_r\right)+\frac{1}{2r^2}\left(\left(\frac{\partial U_r}{\partial\theta}-U_\theta\right)^2+\left(\frac{\partial U_\theta}{\partial\theta}+U_r\right)^2+\left(\frac{\partial U_\alpha}{\partial\theta}\right)^2\right)$$

$$2\varepsilon_{\theta\alpha}=2\varepsilon_{\alpha\theta}=\frac{1}{\left(R_t+r\sin(\theta)\right)}\left(\frac{\partial U_\theta}{\partial\alpha}-U_\alpha\cos(\theta)\right)+\left(\frac{1}{r}\frac{\partial U_\alpha}{\partial\theta}\right)+\frac{1}{r\left(R_t+r\sin(\theta)\right)}\left(\frac{\partial U_r}{\partial\theta}-U_\theta\right)\left(\frac{\partial U_r}{\partial\alpha}-U_\alpha\sin(\theta)\right)+\frac{1}{r\left(R_t+r\sin(\theta)\right)}\left(\frac{\partial U_\theta}{\partial\theta}+U_r\right)\left(\frac{\partial U_\theta}{\partial\alpha}-U_\alpha\cos(\theta)\right)+\frac{1}{r\left(R_t+r\sin(\theta)\right)}\left(\frac{\partial U_\alpha}{\partial\theta}\right)\left(U_r\sin(\theta)+U_\theta\cos(\theta)+\frac{\partial U_\alpha}{\partial\alpha}\right)\tag{13}$$

$$\varepsilon_{\alpha\alpha}=\frac{1}{\left(R_t+r\sin(\theta)\right)}\left(U_r\sin(\theta)+U_\theta\cos(\theta)+\frac{\partial U_\alpha}{\partial\alpha}\right)+\frac{1}{2\left(R_t+r\sin(\theta)\right)^2}\left(\left(\frac{\partial U_r}{\partial\alpha}-U_\alpha\sin(\theta)\right)^2+\left(\frac{\partial U_\theta}{\partial\alpha}-U_\alpha\cos(\theta)\right)^2+\left(U_r\sin(\theta)+U_\theta\cos(\theta)+\frac{\partial U_\alpha}{\partial\alpha}\right)^2\right)$$

Non-linear values in strain field that are in the direction of U_α and U_θ will have little effect on the obtained results, and only non-linear values produced by U_r-dependent parameters can be considered. These assumptions are based on von Kármán's non-linear strains. Therefore, non-linear values in which the parameters U_α and U_θ are existed will be omitted as follows.

$$\varepsilon_{rr}=\left(\frac{\partial U_r}{\partial r}\right)+\frac{1}{2}\left(\frac{\partial U_r}{\partial r}\right)^2$$

$$2\varepsilon_{r\theta}=2\varepsilon_{\theta r}=\frac{1}{r}\left(\frac{\partial U_r}{\partial \theta}-U_\theta\right)+\left(\frac{\partial U_\theta}{\partial r}\right)+\frac{1}{r}\left(\frac{\partial U_r}{\partial r}\right)\left(\frac{\partial U_r}{\partial \theta}\right)$$

$$2\varepsilon_{r\alpha}=2\varepsilon_{\alpha r}=\frac{1}{\left(R_t+r\sin(\theta)\right)}\left(\frac{\partial U_r}{\partial \alpha}-U_\alpha\sin(\theta)\right)+\left(\frac{\partial U_\alpha}{\partial r}\right)+\frac{1}{\left(R_t+r\sin(\theta)\right)}\left(\frac{\partial U_r}{\partial r}\right)\left(\frac{\partial U_r}{\partial \alpha}\right)$$

$$\varepsilon_{\theta\theta}=\frac{1}{r}\left(\frac{\partial U_\theta}{\partial \theta}+U_r\right)+\frac{1}{2r^2}\left(\left(\frac{\partial U_r}{\partial \theta}\right)^2+U_r^2\right)$$

$$2\varepsilon_{\theta\alpha}=2\varepsilon_{\alpha\theta}=\frac{1}{\left(R_t+r\sin(\theta)\right)}\left(\frac{\partial U_\theta}{\partial \alpha}-U_\alpha\cos(\theta)\right)+\left(\frac{1}{r}\frac{\partial U_\alpha}{\partial \theta}\right)+\frac{1}{r\left(R_t+r\sin(\theta)\right)}\left(\frac{\partial U_r}{\partial \theta}\right)$$
$$\left(\frac{\partial U_r}{\partial \alpha}\right)$$

$$\varepsilon_{\alpha\alpha}=\frac{1}{\left(R_t+r\sin(\theta)\right)}\left(U_r\sin(\theta)+U_\theta\cos(\theta)+\frac{\partial U_\alpha}{\partial \alpha}\right)+\frac{1}{2\left(R_t+r\sin(\theta)\right)^2}\left(\left(\frac{\partial U_r}{\partial \alpha}\right)^2\right.$$
$$\left.+\left(U_r\sin(\theta)\right)^2\right) \tag{14}$$

Using the energy method and the principle of minimum potential energy, the governing equations of the torus shape structure can be obtained. According to this principle, the energy variations of the system should be equal to zero. The main relation in this method is introduced as the following equation.

$$\delta\Pi=\delta U_\varepsilon+\delta F_{ext}+\delta K_{ken}=0 \tag{15}$$

In the above equation, δU_ε, δF_{ext} and δK_{ken} are the energy generated by the strains, external loads and kinetics respectively which can be seen in the following equations (t is the time-dependent variable).

$$\delta U_\varepsilon=\int_0^t\left(\iiint_V \sigma_{ij}\delta\varepsilon_{ij}\right)dt \quad i,j=r,\theta,\alpha \quad \left(\text{V is the volume}\right)\left(dV=r\left(R_t+r\sin(\theta)\right)drd\theta d\alpha\right)$$

$$\delta F_{ext}=\int_0^t\left(-\iint_A q_z\left(\delta U_r\right)dA\right)dt \qquad \left(\text{A is the area}\right)\left(dA=r\left(R_t+r\sin(\theta)\right)d\theta d\alpha\right) \tag{16}$$

$$\delta K_{ken}=-\frac{\delta}{2}\int_0^t\left(\iiint_V \rho\left(\left(\frac{\partial U_r}{\partial t}\right)^2+\left(\frac{\partial U_\theta}{\partial t}\right)^2+\left(\frac{\partial U_\alpha}{\partial t}\right)^2\right)dV\right)dt$$

If it is considered the transitional and rotational variable speeds around r, θ and α directions as $\dot{r} = \frac{\partial r}{\partial t}$, $\ddot{r} = \frac{\partial^2 r}{\partial t^2}$, $\dot{\theta} = \frac{\partial \theta}{\partial t}$, $\ddot{\theta} = \frac{\partial^2 \theta}{\partial t^2}$, $\dot{\alpha} = \frac{\partial \alpha}{\partial t}$ and $\ddot{\alpha} = \frac{\partial^2 \alpha}{\partial t^2}$ the accelerations in Toroidal coordinate system can be formulated in below:

$$a_r = \ddot{r} - r\dot{\theta}^2 - r\sin^2(\theta)\dot{\alpha}^2 \tag{17}$$

$$a_\theta = r\ddot{\theta} + 2\dot{r}\dot{\theta} - r\dot{\theta}^2\sin(\theta)\cos(\theta) \tag{18}$$

$$a_\alpha = r\ddot{\alpha}\sin(\theta) + 2\dot{r}\dot{\alpha}\sin(\theta) + 2r\dot{\theta}\dot{\alpha}\cos(\theta) \tag{19}$$

Consequently, the energy generated by acceleration rotation of toroidal structure can be formulated as follow (ρ is the density of the structure's material in kg/m^3):

$$\delta K_{accel} = -\int_0^t \left(\iiint_v \rho r \left(\left(\ddot{\theta} - \dot{\theta}^2 \sin(\theta)\cos(\theta) \right) \delta U_\theta + \left(\ddot{\alpha}\sin(\theta) + 2\dot{\theta}\dot{\alpha}\cos(\theta) \right) \delta U_\alpha - \left(\dot{\theta}^2 + \dot{\alpha}^2 \sin^2(\theta) \right) \delta U_r \right) dV \right) dt \tag{20}$$

The extension of the above integral equations can be rewritten as the following equations. As can be seen, the two integrals above are on volume and surface. Volume and surface changes (dV and dA) can be obtained according to the geometric shape of the Torus structure (Fig. 2) and the following equations will be obtained by substituting and expanding the indices.

$$\delta U_\varepsilon = \int_0^t \left(\iiint_V \left(\sigma_{rr}\delta\varepsilon_{rr} + \sigma_{r\theta}\delta\varepsilon_{r\theta} + \sigma_{r\alpha}\delta\varepsilon_{r\alpha} + \sigma_{\theta r}\delta\varepsilon_{\theta r} + \sigma_{\theta\theta}\delta\varepsilon_{\theta\theta} + \sigma_{\theta\alpha}\delta\varepsilon_{\theta\alpha} + \sigma_{\alpha r}\delta\varepsilon_{\alpha r} + \sigma_{\alpha\theta}\delta\varepsilon_{\alpha\theta} + \sigma_{\alpha\alpha}\delta\varepsilon_{\alpha\alpha} \right) dV \right) dt \tag{21}$$

δU_ε integral equation should be further expanded and the strain changes ($\delta\varepsilon_{ij}(i,j = r,\theta,\alpha)$) presented in matrix 13 should be substituted in Eq. (21). The strain matrix 13 is a general matrix. In other words, any desired value can be considered for the displacement field (U_r, U_θ and U_α).

In this study, the first-order shear deformation theory (FSDT) has been used due to the many advantages and simple formulations. One of the advantages of the first-order shear deformation theory is the provision of accurate results for moderately thick structures. The distribution of shear force along the thickness in this displacement field (FSDT) is considered linearly. As an innovation presented in this study, it can be mentioned the strain matrix (matrix 13) in general form, and according to this matrix, any type of displacement field can be considered and derive the governing equations based on arbitrary considered displacement field. In other words, the researcher can apply quasi-three-dimensional displacement theories in matrix 13 and derive the resulted quasi-three-dimensional governing equations. So, it is possible to examine conveniently the effects of strain changes along thickness. Therefore, this research can be a benchmark reference for researchers who is studying the analysis of mechanical properties of torus-shaped structures. Whereas deriving the governing equations in Toroidal coordinate system has been explained carefully in details, readers can apply the proposed method for any kind of coordinate system and in consequence analyze many other structures. The basic equations of the first-order shear deformation theory for a torus structure will be the following three equations.

$$\begin{aligned} U_{\alpha}(r,\theta,\alpha,t) &= u_0(\theta,\alpha,t) + r\psi_1(\theta,\alpha,t) \\ U_{\theta}(r,\theta,\alpha,t) &= v_0(\theta,\alpha,t) + r\psi_2(\theta,\alpha,t) \\ U_{r}(r,\theta,\alpha,t) &= w_0(\theta,\alpha,t) \end{aligned} \tag{22}$$

Variations along the r direction is considered as z direction through the thickness of structure. As mentioned earlier, the smaller radius of ring torus is considered to be a constant value as R (Fig. 2). According to the displacement field (Eq. (22)), it is expected that the third-order partial differential equations (PDE) will be derived due to three independent variables θ, α, t. So, the presented displacement field (Eq. (22)) is rewritten as follows:

$$
\begin{aligned}
U_{\alpha}(z,\theta,\alpha,t) &= u_0(\theta,\alpha,t) + z\,\psi_1(\theta,\alpha,t) \\
U_{\theta}(z,\theta,\alpha,t) &= v_0(\theta,\alpha,t) + z\,\psi_2(\theta,\alpha,t) \\
U_{z}(z,\theta,\alpha,t) &= w_0(\theta,\alpha,t)
\end{aligned}
\tag{23}
$$

In the above equations, as mentioned earlier, U_α, U_θ, and U_z are displacements in the three independent directions of the Toroidal coordinate system (the three main directions of α, θ, and z) in which their definitions are considered linearly. The values of $u_0(\theta,\alpha,t)$, $v_0(\theta,\alpha,t)$, and $w_0(\theta,\alpha,t)$ show the transition changes along the three directions of θ, α, and z. Also, $\psi_1(\theta,\alpha,t)$ and $\psi_2(\theta,\alpha,t)$ are the rotational functions around α and θ directions respectively. The variable z also represents changes through the thickness. The values of variations δU_α, δU_θ and $\delta U_r = \delta U_z$ can now be calculated and substituted in Eq. (16) according to the following equations.

$$
\begin{aligned}
\delta U_{\alpha}(z,\theta,\alpha,t) &= \delta u_0(\theta,\alpha,t) + z\,\delta\psi_1(\theta,\alpha,t) \\
\delta U_{\theta}(z,\theta,\alpha,t) &= \delta v_0(\theta,\alpha,t) + z\,\delta\psi_2(\theta,\alpha,t) \\
\delta U_{r}(r,\theta,\alpha,t) &= \delta U_{z}(z,\theta,\alpha,t) = \delta w_0(\theta,\alpha,t)
\end{aligned}
\tag{24}
$$

By substituting the above equations (Eq. (23)), the strain components in Eq. (14) can be rewritten as the following expressions.

$$\varepsilon_{zz} = \left(\frac{\partial U_z}{\partial z}\right) + \frac{1}{2}\left(\frac{\partial U_z}{\partial z}\right)^2 = 0$$

$$2\varepsilon_{z\theta} = 2\varepsilon_{\theta z} = \frac{1}{R}\left(\frac{\partial U_z}{\partial \theta} - U_\theta\right) + \left(\frac{\partial U_\theta}{\partial z}\right) + \frac{1}{R}\left(\frac{\partial U_z}{\partial z}\right)\left(\frac{\partial U_z}{\partial \theta}\right) = \frac{1}{R}\left(\frac{\partial w_0}{\partial \theta} - \left(v_0 + z\,\psi_2\right)\right) + \psi_2$$

$$2\varepsilon_{z\alpha} = 2\varepsilon_{\alpha z} = \frac{1}{\left(R_t + R\sin(\theta)\right)}\left(\frac{\partial U_z}{\partial \alpha} - U_\alpha \sin(\theta)\right) + \left(\frac{\partial U_\alpha}{\partial z}\right) + \frac{1}{\left(R_t + R\sin(\theta)\right)}\left(\frac{\partial U_z}{\partial z}\right)\left(\frac{\partial U_z}{\partial \alpha}\right)$$

$$= \frac{1}{\left(R_t + R\sin(\theta)\right)}\left(\frac{\partial w_0}{\partial \alpha} - \left(u_0 + z\,\psi_1\right)\sin(\theta)\right) + \psi_1$$

$$\varepsilon_{\theta\theta} = \frac{1}{R}\left(\frac{\partial U_\theta}{\partial \theta} + U_z\right) + \frac{1}{2R^2}\left(\left(\frac{\partial U_z}{\partial \theta}\right)^2 + U_z^2\right) = \frac{1}{R}\left(\frac{\partial v_0}{\partial \theta} + z\,\frac{\partial \psi_2}{\partial \theta} + w_0\right) + \frac{1}{2R^2}\left(\left(\frac{\partial w_0}{\partial \theta}\right)^2 + w_0^2\right)$$

$$2\varepsilon_{\theta\alpha} = 2\varepsilon_{\alpha\theta} = \frac{1}{\left(R_t + R\sin(\theta)\right)}\left(\frac{\partial U_\theta}{\partial \alpha} - U_\alpha \cos(\theta)\right) + \left(\frac{1}{R}\frac{\partial U_\alpha}{\partial \theta}\right) + \frac{1}{R\left(R_t + R\sin(\theta)\right)}\left(\frac{\partial U_z}{\partial \theta}\right)$$

$$\left(\frac{\partial U_z}{\partial \alpha}\right) = \frac{1}{\left(R_t + R\sin(\theta)\right)}\left(\frac{\partial v_0}{\partial \alpha} + z\,\frac{\partial \psi_2}{\partial \alpha} - \left(u_0 + z\,\psi_1\right)\cos(\theta)\right) + \frac{1}{R}\left(\frac{\partial u_0}{\partial \theta} + z\,\frac{\partial \psi_1}{\partial \theta}\right)$$

$$+ \frac{1}{R\left(R_t + R\sin(\theta)\right)}\left(\frac{\partial w_0}{\partial \theta}\right)\left(\frac{\partial w_0}{\partial \alpha}\right)$$

$$\varepsilon_{\alpha\alpha} = \frac{1}{\left(R_t + R\sin(\theta)\right)}\left(U_z \sin(\theta) + U_\theta \cos(\theta) + \frac{\partial U_\alpha}{\partial \alpha}\right) + \frac{1}{2\left(R_t + R\sin(\theta)\right)^2}\left(\left(\frac{\partial U_z}{\partial \alpha}\right)^2\right. \tag{25}$$

$$\left. + \left(U_z \sin(\theta)\right)^2\right) = \frac{1}{\left(R_t + R\sin(\theta)\right)}\left(w_0 \sin(\theta) + \left(v_0 + z\,\psi_2\right)\cos(\theta) + \frac{\partial u_0}{\partial \alpha} + z\,\frac{\partial \psi_1}{\partial \alpha}\right) +$$

$$\frac{1}{2\left(R_t + R\sin(\theta)\right)^2}\left(\left(\frac{\partial w_0}{\partial \alpha}\right)^2 + \left(w_0 \sin(\theta)\right)^2\right)$$

Considering the strain components (Eq. (25)) and substituting the strain variations into Eq. (21), the expansion of Eq. (21) is expressed in below.

$$\delta U_{\varepsilon} = \int_0^t \Bigg(\iiint_V \left(\sigma_{zz}\delta\varepsilon_{zz} + \sigma_{z\theta}\delta\varepsilon_{z\theta} + \sigma_{z\alpha}\delta\varepsilon_{z\alpha} + \sigma_{\theta z}\delta\varepsilon_{\theta z} + \sigma_{\theta\theta}\delta\varepsilon_{\theta\theta} + \sigma_{\theta\alpha}\delta\varepsilon_{\theta\alpha} \right.$$

$$\left. + \sigma_{\alpha z}\delta\varepsilon_{\alpha z} + \sigma_{\alpha\theta}\delta\varepsilon_{\alpha\theta} + \sigma_{\alpha\alpha}\delta\varepsilon_{\alpha\alpha} \right) dV \Bigg) dt =$$

$$= \int_0^t \Bigg(\iiint_V \left(\sigma_{zz}\delta\varepsilon_{zz} + \sigma_{\alpha\alpha}\delta\varepsilon_{\alpha\alpha} + \sigma_{\theta\theta}\delta\varepsilon_{\theta\theta} + 2\sigma_{z\theta}\delta\varepsilon_{z\theta} + 2\sigma_{z\alpha}\delta\varepsilon_{z\alpha} + 2\sigma_{\theta\alpha}\delta\varepsilon_{\theta\alpha} \right) dV \Bigg) dt =$$

$$\int_0^t \Bigg(\int_0^{\alpha} \int_0^{\theta} \int_{-\frac{h}{2}}^{\frac{h}{2}} \Bigg(\sigma_{\alpha\alpha} \Bigg(\frac{1}{\left(R_t + R\sin(\theta)\right)} \Bigg(\delta w_0 \sin(\theta) + \left(\delta v_0 + z\delta\psi_2\right)\cos(\theta) + \frac{\partial \delta u_0}{\partial \alpha} + z\frac{\partial \delta\psi_1}{\partial \alpha} \Bigg) +$$

$$\frac{1}{\left(R_t + R\sin(\theta)\right)^2} \Bigg(\left(\frac{\partial \delta w_0}{\partial \alpha}\right)\left(\frac{\partial w_0}{\partial \alpha}\right) + w_0\left(\delta w_0 \sin^2(\theta)\right) \Bigg) \Bigg) + \sigma_{\theta\theta} \Bigg(\frac{1}{R} \Bigg(\frac{\partial \delta v_0}{\partial \theta} + z\frac{\partial \delta\psi_2}{\partial \theta} + \delta w_0 \Bigg)$$

$$+ \frac{1}{R^2} \Bigg(\left(\frac{\partial \delta w_0}{\partial \theta}\right)\left(\frac{\partial w_0}{\partial \theta}\right) + w_0\delta w_0 \Bigg) \Bigg) + \sigma_{z\theta} \Bigg(\frac{1}{R} \Bigg(\frac{\partial \delta w_0}{\partial \theta} - \left(\delta v_0 + z\delta\psi_2\right) \Bigg) + \delta\psi_2 \Bigg) +$$

$$\sigma_{z\alpha} \Bigg(\frac{1}{\left(R_t + R\sin(\theta)\right)} \Bigg(\frac{\partial \delta w_0}{\partial \alpha} - \left(\delta u_0 + z\delta\psi_1\right)\sin(\theta) \Bigg) + \delta\psi_1 \Bigg) + \sigma_{\theta\alpha} \Bigg(\frac{1}{\left(R_t + R\sin(\theta)\right)} \Bigg(\frac{\partial \delta v_0}{\partial \alpha}$$

$$+ z\frac{\partial \delta\psi_2}{\partial \alpha} - \left(\delta u_0 + z\delta\psi_1\right)\cos(\theta) \Bigg) + \frac{1}{R} \Bigg(\frac{\partial \delta u_0}{\partial \theta} + z\frac{\partial \delta\psi_1}{\partial \theta} \Bigg) + \frac{1}{R\left(R_t + R\sin(\theta)\right)} \Bigg(\Bigg(\frac{\partial \delta w_0}{\partial \theta} \Bigg) \tag{26}$$

$$\left(\frac{\partial w_0}{\partial \alpha}\right) + \left(\frac{\partial w_0}{\partial \theta}\right)\left(\frac{\partial \delta w_0}{\partial \alpha}\right) \Bigg) \Bigg) \Bigg) \Bigg) R\left(R_t + R\sin(\theta)\right) dz d\alpha d\theta \Bigg) dt$$

In the above equation, it was assumed that $\sigma_{ij} = \sigma_{ji}$. For example, $\sigma_{z\theta} = \sigma_{\theta z}$, $\sigma_{\theta\alpha} = \sigma_{\alpha\theta}$ and etc.

By integrating Eq. (26) in the direction of z and expressing the definition of momentum and stress resultants as the following equations ($N_{ij}(i,j=\alpha,\theta)$, $M_{ij}(i,j=z,\alpha,\theta)$, $Q_{ij}(i,j=z,\alpha,\theta)$), Eq. (26) can finally be rewritten as follows:

$$
\begin{aligned}
&\int_0^t \Bigg(\int_0^\alpha \int_0^\theta R \Bigg(N_{\alpha\alpha}\delta w_0 \sin(\theta) + \left(N_{\alpha\alpha}\delta v_0 + M_{\alpha\alpha}\delta\psi_2\right)\cos(\theta) + N_{\alpha\alpha}\frac{\partial \delta u_0}{\partial \alpha} + M_{\alpha\alpha}\frac{\partial \delta\psi_1}{\partial \alpha} \Bigg) \\
&+ \frac{R}{\left(R_t + R\sin(\theta)\right)} \Bigg(N_{\alpha\alpha}\left(\frac{\partial \delta w_0}{\partial \alpha}\right)\left(\frac{\partial w_0}{\partial \alpha}\right) + N_{\alpha\alpha}w_0\left(\delta w_0 \sin^2(\theta)\right) \Bigg) + \left(R_t + R\sin(\theta)\right) \\
&\left(N_{\theta\theta}\frac{\partial \delta v_0}{\partial \theta} + M_{\theta\theta}\frac{\partial \delta\psi_2}{\partial \theta} + N_{\theta\theta}\delta w_0 \right) + \frac{N_{\theta\theta}\left(R_t + R\sin(\theta)\right)}{R}\left(\left(\frac{\partial \delta w_0}{\partial \theta}\right)\left(\frac{\partial w_0}{\partial \theta}\right) + w_0\delta w_0 \right) \\
&+ \left(R_t + R\sin(\theta)\right)\left(Q_{z\theta}\frac{\partial \delta w_0}{\partial \theta} - \left(Q_{z\theta}\delta v_0 + M_{z\theta}\delta\psi_2\right) \right) + R\left(R_t + R\sin(\theta)\right)Q_{z\theta}\delta\psi_2 \\
&+ R\left(Q_{z\alpha}\frac{\partial \delta w_0}{\partial \alpha} - \left(Q_{z\alpha}\delta u_0 + M_{z\alpha}\delta\psi_1\right)\sin(\theta) \right) + R\left(R_t + R\sin(\theta)\right)Q_{z\alpha}\delta\psi_1 \\
&+ R\left(N_{\theta\alpha}\frac{\partial \delta v_0}{\partial \alpha} + M_{\theta\alpha}\frac{\partial \delta\psi_2}{\partial \alpha} - \left(N_{\theta\alpha}\delta u_0 + M_{\theta\alpha}\delta\psi_1\right)\cos(\theta) \right) + \left(R_t + R\sin(\theta)\right) \\
&\left(N_{\theta\alpha}\frac{\partial \delta u_0}{\partial \theta} + M_{\theta\alpha}\frac{\partial \delta\psi_1}{\partial \theta} \right) + N_{\theta\alpha}\left(\left(\frac{\partial \delta w_0}{\partial \theta}\right)\left(\frac{\partial w_0}{\partial \alpha}\right) + \left(\frac{\partial w_0}{\partial \theta}\right)\left(\frac{\partial \delta w_0}{\partial \alpha}\right) \right) d\alpha d\theta \Bigg) dt \\
&\left(N_{\alpha\alpha}, N_{\alpha\theta}, N_{\theta\theta}\right) = \int_{-\frac{h}{2}}^{\frac{h}{2}} \left(\sigma_{\alpha\alpha}, \sigma_{\alpha\theta}, \sigma_{\theta\theta}\right) dz \,; \left(Q_{z\theta}, Q_{z\alpha}\right) = \int_{-\frac{h}{2}}^{\frac{h}{2}} \left(\sigma_{z\theta}, \sigma_{z\alpha}\right) dz \,; \\
&\left(M_{\alpha\alpha}, M_{\alpha\theta}, M_{\theta\theta}, M_{z\theta}, M_{z\alpha}\right) = \int_{-\frac{h}{2}}^{\frac{h}{2}} \left(\sigma_{\alpha\alpha}, \sigma_{\alpha\theta}, \sigma_{\theta\theta}, \sigma_{z\theta}, \sigma_{z\alpha}\right) z dz
\end{aligned}
\tag{27}
$$

Some of the integrals made in Eq. (27) are integrals by part. For example, the method of calculating one of these types of integrals can be considered as the following process

$$
\begin{aligned}
&\int u dv = uv - \int v du \\
&\iint_A RN_{\alpha\alpha} \underbrace{\frac{\partial \delta u_0}{\partial \alpha} d\alpha d\theta}_{u \quad dv} = RN_{\alpha\alpha}\delta u_0 \Big]_0^\alpha - \int_0^\alpha \int_0^\theta \frac{\partial}{\partial \alpha}\left(RN_{\alpha\alpha}\right)\delta u_0 d\alpha d\theta
\end{aligned}
\tag{28}
$$

The calculation of other integrals in Eq. (16) is presented as follows

$$\delta K_{ken} = -\frac{\delta}{2}\int_0^t \left(\iiint_V \rho \left(\left(\frac{\partial U_\theta}{\partial t} \right)^2 + \left(\frac{\partial U_\alpha}{\partial t} \right)^2 + \left(\frac{\partial U_r}{\partial t} \right)^2 \right) dV \right) dt$$

$$= -\int_0^t \left(\iiint_V \rho \left(\left(\frac{\partial U_\theta}{\partial t}\frac{\partial \delta U_\theta}{\partial t} \right) + \left(\frac{\partial U_\alpha}{\partial t}\frac{\partial \delta U_\alpha}{\partial t} \right) + \left(\frac{\partial U_z}{\partial t}\frac{\partial \delta U_z}{\partial t} \right) \right) dV \right) dt =$$

$$= -\int_0^t \left(\iiint_V \rho \left(\left(\frac{\partial u_0}{\partial t} + z\frac{\partial \psi_1}{\partial t} \right)\left(\frac{\partial \delta u_0}{\partial t} + z\frac{\partial \delta \psi_1}{\partial t} \right) + \left(\frac{\partial v_0}{\partial t} + z\frac{\partial \psi_2}{\partial t} \right)\left(\frac{\partial \delta v_0}{\partial t} + z\frac{\partial \delta \psi_2}{\partial t} \right) \right. \right.$$

$$\left. \left. + \left(\frac{\partial w_0}{\partial t}\frac{\partial \delta w_0}{\partial t} \right) \right) dV \right) dt = -\int_0^t \left(\iint_A \left(I_1 \left(\frac{\partial u_0}{\partial t}\frac{\partial \delta u_0}{\partial t} \right) + I_2 \left(\frac{\partial u_0}{\partial t}\frac{\partial \delta \psi_1}{\partial t} + \frac{\partial \psi_1}{\partial t}\frac{\partial \delta u_0}{\partial t} \right) \right. \right. \tag{29}$$

$$+ I_3 \left(\frac{\partial \psi_1}{\partial t}\frac{\partial \delta \psi_1}{\partial t} \right) + I_1 \left(\frac{\partial v_0}{\partial t}\frac{\partial \delta v_0}{\partial t} \right) + I_2 \left(\frac{\partial v_0}{\partial t}\frac{\partial \delta \psi_2}{\partial t} + \frac{\partial \psi_2}{\partial t}\frac{\partial \delta v_0}{\partial t} \right) + I_3 \left(\frac{\partial \psi_2}{\partial t}\frac{\partial \delta \psi_2}{\partial t} \right)$$

$$\left. \left. + I_1 \left(\frac{\partial w_0}{\partial t}\frac{\partial \delta w_0}{\partial t} \right) \right) R\left(R_t + R\sin(\theta) \right) d\theta d\alpha \right) dt \qquad (I_1, I_2, I_3) = \int_{-\frac{h}{2}}^{\frac{h}{2}} \rho\left(1, z, z^2\right) dz$$

$$\delta K_{accel} = -\int_0^t \left(\iiint_v \rho r \left(\left(\ddot{\theta} - \dot{\theta}^2 \sin(\theta)\cos(\theta) \right)\delta U_\theta + \left(\ddot{\alpha}\sin(\theta) + 2\dot{\theta}\dot{\alpha}\cos(\theta) \right)\delta U_\alpha \right. \right.$$

$$\left. \left. - \left(\dot{\theta}^2 + \dot{\alpha}^2 \sin^2(\theta) \right)\delta U_r \right) dV \right) dt = \tag{30}$$

$$-\int_0^t \left(\iint_A I_1 R \left(\left(\ddot{\theta} - \dot{\theta}^2 \sin(\theta)\cos(\theta) \right)\delta u_0 + \left(\ddot{\alpha}\sin(\theta) + 2\dot{\theta}\dot{\alpha}\cos(\theta) \right)\delta v_0 \right. \right.$$

$$\left. \left. - \left(\dot{\theta}^2 + \dot{\alpha}^2 \sin^2(\theta) \right)\delta w_0 \right) R\left(R_t + R\sin(\theta) \right) d\theta d\alpha \right) dt$$

Now, by adding the values of the changes in the directions δu_0, δv_0, δw_0, $\delta \psi_1$ and $\delta \psi_2$, the dynamical governing equations of a ring torus-shaped structure can be obtained as the following equations

$$\delta u_0 : \frac{\partial N_{\alpha\alpha}}{\partial \alpha} + \sin(\theta) Q_{z\alpha} + 2\cos(\theta) N_{\theta\alpha} + \left(\frac{R_t}{R} + \sin(\theta) \right)\frac{\partial N_{\theta\alpha}}{\partial \theta} +$$

$$\left(R_t + R\sin(\theta) \right)\left(I_1 R \left(\ddot{\theta} - \dot{\theta}^2 \sin(\theta)\cos(\theta) \right) + \left(I_1 \frac{\partial^2 u_0}{\partial t^2} + I_2 \frac{\partial^2 \psi_1}{\partial t^2} \right) \right) = 0 \tag{31}$$

$$\delta v_0 : \left(\frac{R_t}{R} + \sin(\theta) \right) Q_{z\theta} + \cos(\theta)\left(N_{\theta\theta} - N_{\alpha\alpha} \right) + \left(\frac{R_t}{R} + \sin(\theta) \right)\frac{\partial N_{\theta\theta}}{\partial \theta} + \frac{\partial N_{\theta\alpha}}{\partial \alpha} +$$

$$\left(R_t + R\sin(\theta) \right)\left(I_1 R \left(\ddot{\alpha}\sin(\theta) + 2\dot{\theta}\dot{\alpha}\cos(\theta) \right) + \left(I_1 \frac{\partial^2 v_0}{\partial t^2} + I_2 \frac{\partial^2 \psi_2}{\partial t^2} \right) \right) = 0 \tag{32}$$

$$\delta w_0 : \cos(\theta) Q_{z\theta} + \left(\frac{R_t}{R} + \sin(\theta)\right)\frac{\partial Q_{z\theta}}{\partial \theta} + \frac{\partial Q_{z\alpha}}{\partial \alpha} - \left(\frac{R_t}{R} + \sin(\theta)\right) N_{\theta\theta} - \sin(\theta) N_{\alpha\alpha}$$
$$+ \frac{1}{R}\frac{\partial}{\partial \theta}\left(\left(\frac{R_t}{R} + \sin(\theta)\right) N_{\theta\theta}\frac{\partial N_{\theta\theta}}{\partial \theta}\right) - \frac{1}{R}\left(\frac{R_t}{R} + \sin(\theta)\right) N_{\theta\theta} w_0 + \frac{1}{R}\frac{\partial}{\partial \theta}\left(N_{\theta\alpha}\frac{\partial w_0}{\partial \alpha}\right) +$$
$$\frac{1}{R}\frac{\partial}{\partial \alpha}\left(N_{\theta\alpha}\frac{\partial w_0}{\partial \theta}\right) + \frac{1}{R\left(\frac{R_t}{R} + \sin(\theta)\right)}\frac{\partial}{\partial \alpha}\left(N_{\alpha\alpha}\frac{\partial w_0}{\partial \alpha}\right) - \frac{1}{R\left(\frac{R_t}{R} + \sin(\theta)\right)}\left(N_{\alpha\alpha} w_0 \left(\sin(\theta)\right)^2\right) \quad (33)$$
$$+ \left(R_t + R\sin(\theta)\right)\left(q_r - I_1 R\left(\dot{\theta}^2 + \dot{\alpha}^2 \sin^2(\theta)\right) + I_1 \frac{\partial^2 w_0}{\partial t^2}\right) = 0$$

$$\delta \psi_1 : \frac{\partial M_{\alpha\alpha}}{\partial \alpha} - \left(R_t + R\sin(\theta)\right) Q_{z\alpha} + 2\cos(\theta) M_{\theta\alpha} + \left(\frac{R_t}{R} + \sin(\theta)\right)\frac{\partial M_{\theta\alpha}}{\partial \theta} + \sin(\theta) M_{z\alpha} \quad (34)$$
$$+ \left(R_t + R\sin(\theta)\right)\left(I_2 \frac{\partial^2 u_0}{\partial t^2} + I_3 \frac{\partial^2 \psi_1}{\partial t^2}\right) = 0$$

$$\delta \psi_2 : \left(\frac{R_t}{R} + \sin(\theta)\right) M_{z\theta} + \cos(\theta)\left(M_{\theta\theta} - M_{\alpha\alpha}\right) + \left(R_t + R\sin(\theta)\right) Q_{z\theta} + \left(\frac{R_t}{R} + \sin(\theta)\right)\frac{\partial M_{\theta\theta}}{\partial \theta} \quad (35)$$
$$- \frac{\partial M_{\theta\alpha}}{\partial \alpha} + \left(R_t + R\sin(\theta)\right)\left(I_2 \frac{\partial^2 v_0}{\partial t^2} + I_3 \frac{\partial^2 \psi_2}{\partial t^2}\right) = 0$$

4. Dynamic analysis of cylindrical-shaped structure

According to the method mentioned for obtaining the dynamic governing equations of the torus structure, which was fully explained in details in the previous section, the governing equations of the cylindrical structure can also be obtained. The schematic view of the rotating cylindrical structure can be seen in Fig. 4. The structure is under the internal pressure q_r and also the hygro-thermal environment is considered. The height of the cylinder is L. The cylinder is rotating around central axis AX_θ with angular velocity and acceleration $\dot{\theta}$ and $\ddot{\theta}$ respectively. The acceleration vector is $\vec{a} = \left(\ddot{r} - r\dot{\theta}^2\right)\hat{e}_r + \left(r\ddot{\theta} + 2\dot{r}\dot{\theta}\right)\hat{e}_\theta + (\ddot{z})\hat{e}_z$. Variations of radius and height per time $(\dot{r}, \dot{z})$ are neglectable and it can be assumed that $\dot{r} = \ddot{r} = \dot{z} = \ddot{z} = 0$. In this section, only the strain matrix and the final governing equations are written according to the following equations

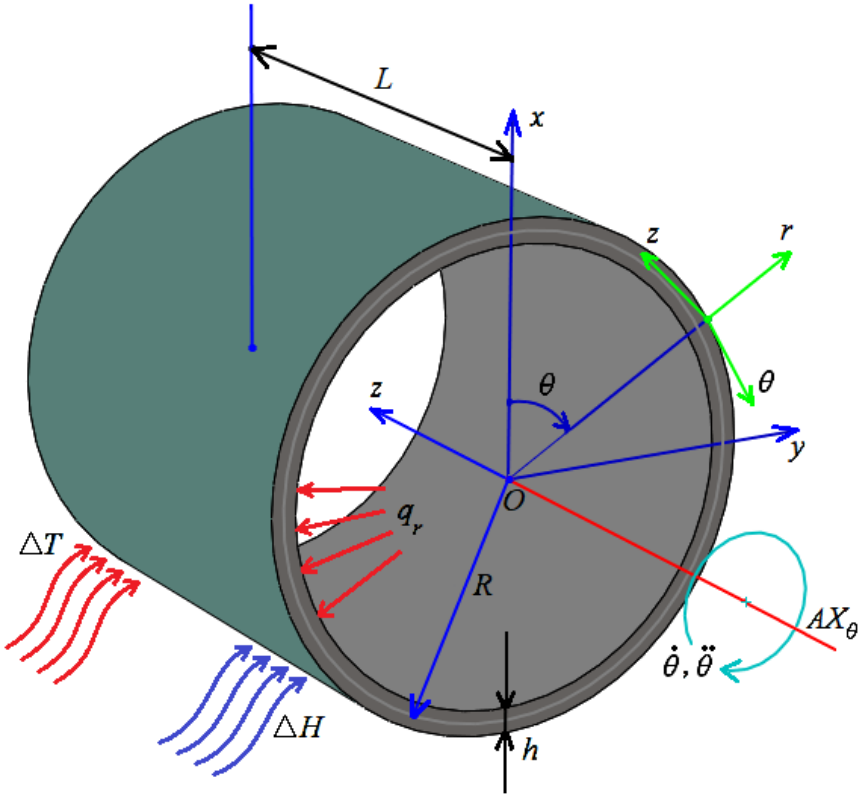

Fig. 4. Schematic view of rotating cylindrical structure

$$\varepsilon_{ij}=\begin{bmatrix}\varepsilon_{rr} & \varepsilon_{r\theta} & \varepsilon_{rz}\\ \varepsilon_{\theta r} & \varepsilon_{\theta\theta} & \varepsilon_{\theta z}\\ \varepsilon_{zr} & \varepsilon_{z\theta} & \varepsilon_{zz}\end{bmatrix};\begin{cases}U_\theta(r,\theta,z)=u_0(\theta,z)+r\psi_1(\theta,z)\\ U_z(r,\theta,z)=v_0(\theta,z)+r\psi_2(\theta,z)\\ U_r(r,\theta,z)=w_0(\theta,z)\end{cases}$$

$$\varepsilon_{rr}=0$$

$$2\varepsilon_{r\theta}=2\varepsilon_{\theta r}=\frac{1}{r}\left(\frac{\partial U_r}{\partial\theta}-U_\theta\right)+\left(\frac{\partial U_\theta}{\partial r}\right)=\frac{1}{R}\left(\frac{\partial w_0}{\partial\theta}-u_0-r\psi_1\right)+\psi_1$$

$$2\varepsilon_{rz}=2\varepsilon_{zr}=\left(\frac{\partial U_r}{\partial z}\right)+\left(\frac{\partial U_z}{\partial r}\right)=\frac{\partial w_0}{\partial z}+\psi_2$$

$$\varepsilon_{\theta\theta}=\frac{1}{r}\left(\frac{\partial U_\theta}{\partial\theta}+U_r\right)+\frac{1}{2r^2}\left(\left(\frac{\partial U_r}{\partial\theta}\right)^2+U_r^2\right)=\frac{1}{R}\left(\frac{\partial u_0}{\partial\theta}+r\frac{\partial\psi_1}{\partial\theta}+w_0\right)+\frac{1}{2R^2}\left(\left(\frac{\partial w_0}{\partial\theta}\right)^2+w_0^2\right)$$

$$2\varepsilon_{\theta z}=2\varepsilon_{z\theta}=\frac{1}{r}\left(\frac{\partial U_z}{\partial\theta}\right)+\left(\frac{\partial U_\theta}{\partial z}\right)+\frac{1}{r}\left(\frac{\partial U_r}{\partial\theta}\right)\left(\frac{\partial U_r}{\partial z}\right)=\frac{1}{R}\left(\frac{\partial v_0}{\partial\theta}+r\frac{\partial\psi_2}{\partial\theta}\right)+\left(\frac{\partial u_0}{\partial z}+r\frac{\partial\psi_1}{\partial z}\right)$$
$$+\frac{1}{R}\left(\frac{\partial w_0}{\partial\theta}\right)\left(\frac{\partial w_0}{\partial z}\right)$$

$$\varepsilon_{zz}=\left(\frac{\partial U_z}{\partial z}\right)+\frac{1}{2}\left(\frac{\partial U_r}{\partial z}\right)^2=\frac{\partial v_0}{\partial z}+r\frac{\partial\psi_2}{\partial z}+\frac{1}{2}\left(\frac{\partial w_0}{\partial z}\right)^2 \tag{36}$$

$$\delta u_0 : N_{r\theta} + \frac{\partial N_{\theta\theta}}{\partial \theta} + R\frac{\partial N_{\theta z}}{\partial z} + I_1 R^2 \ddot{\theta} - R\left(I_1 \frac{\partial^2 u_0}{\partial t^2} + I_2 \frac{\partial^2 \psi_1}{\partial t^2}\right) = 0 \tag{37}$$

$$\delta v_0 : \frac{\partial N_{\theta z}}{\partial \theta} - R\frac{\partial N_{zz}}{\partial z} - R\left(I_1 \frac{\partial^2 v_0}{\partial t^2} + I_2 \frac{\partial^2 \psi_2}{\partial t^2}\right) = 0 \tag{38}$$

$$\delta w_0 : \frac{\partial N_{r\theta}}{\partial \theta} - N_{\theta\theta} + R\frac{\partial N_{rz}}{\partial z} + \frac{1}{R}\frac{\partial}{\partial \theta}\left(N_{\theta\theta}\frac{\partial w_0}{\partial \theta}\right) - \frac{1}{R}\left(N_{\theta\theta} w_0\right) + \frac{\partial}{\partial \theta}\left(N_{\theta z}\frac{\partial w_0}{\partial z}\right) + \frac{\partial}{\partial z}\left(N_{\theta z}\frac{\partial w_0}{\partial \theta}\right) + R\frac{\partial}{\partial z}\left(N_{zz}\frac{\partial w_0}{\partial z}\right) + Rq_z - I_1 R^2 \dot{\theta}^2 - I_1 R\frac{\partial^2 w_0}{\partial t^2} = 0 \tag{39}$$

$$\delta \psi_1 : M_{r\theta} - RN_{r\theta} + \frac{\partial M_{\theta\theta}}{\partial \theta} + R\frac{\partial M_{\theta z}}{\partial z} - R\left(I_2 \frac{\partial^2 u_0}{\partial t^2} + I_3 \frac{\partial^2 \psi_1}{\partial t^2}\right) = 0 \tag{40}$$

$$\delta \psi_2 : \frac{\partial M_{\theta z}}{\partial \theta} - RN_{rz} + R\frac{\partial M_{zz}}{\partial z} - R\left(I_2 \frac{\partial^2 v_0}{\partial t^2} + I_3 \frac{\partial^2 \psi_2}{\partial t^2}\right) = 0 \tag{41}$$

If the angular velocity ($\dot{\theta}$) is considered constant and also the internal pressure is symmetrical and uniform, there will be no changes in the direction of θ ($\frac{\partial}{\partial \theta}(f) = U_\theta = 0$). Thus, the governing equations (Eqs. (37-41)) can be reformulated as follows

$$\delta v_0 : \frac{\partial N_{zz}}{\partial z} + \left(I_1 \frac{\partial^2 v_0}{\partial t^2} + I_2 \frac{\partial^2 \psi_2}{\partial t^2}\right) = 0 \tag{42}$$

$$\delta w_0 : R\frac{\partial N_{rz}}{\partial z} - N_{\theta\theta} - \frac{1}{R}\left(N_{\theta\theta} w_0\right) + R\frac{\partial}{\partial z}\left(N_{zz}\frac{\partial w_0}{\partial z}\right) + Rq_z - I_1 R^2 \dot{\theta}^2 - I_1 R\frac{\partial^2 w_0}{\partial t^2} = 0 \tag{43}$$

$$\delta \psi_2 : N_{rz} - \frac{\partial M_{zz}}{\partial z} + \left(I_2 \frac{\partial^2 v_0}{\partial t^2} + I_3 \frac{\partial^2 \psi_2}{\partial t^2}\right) = 0 \tag{44}$$

5. Stress analysis

The Hook definition for stress analysis has been used in this study. The main equation for the stress analysis can be expressed as follow:

$$\sigma = C : \varepsilon$$

$$C = \frac{E(z)}{\left(1-\nu(z)^2\right)} \begin{bmatrix} 1 & \nu(z) & 0 & 0 & 0 & 0 \\ \nu(z) & 1 & 0 & 0 & 0 & 0 \\ 0 & 0 & \frac{1-\nu(z)}{2} & 0 & 0 & 0 \\ 0 & 0 & 0 & \frac{1-\nu(z)}{2} & 0 & 0 \\ 0 & 0 & 0 & 0 & \frac{1-\nu(z)}{2} & 0 \\ 0 & 0 & 0 & 0 & 0 & \frac{1-\nu(z)}{2} \end{bmatrix} \tag{45}$$

In the above relation, σ is the stress generated on the structure, C is the material characteristic matrix and ε is the vector of the strain field.

The material characteristic matrix (matrix C) can be obtained for the FGM material considered in this study. Today, FGM structures have attracted a lot of attention from researchers [26-34]. In functionally graded materials (FGM's), material specifications change in one or more directions. For example, it can be assumed that the properties of material change with respect to thickness. Young's elastic modulus ($E(z)$), Poisson's coefficient ($\nu(z)$), thermal conductivity ($\alpha_T(z)$) and moisture coefficient ($\beta(z)$) can be thought of as a function of thickness that varies from the internal values of E_i, ν_i, α_{Ti} and β_i to the external values of E_o, ν_o,, α_{To} and β_o. Parameter n shows the intensity of changes in material properties from internal to external values. The material properties can be written as the following equations

$$\begin{aligned} E(z) &= (E_o - E_i)\left(\frac{z}{h}+\frac{1}{2}\right)^n + E_i \qquad -\frac{h}{2} \le z \le \frac{h}{2} \\ \nu(z) &= (\nu_o - \nu_i)\left(\frac{z}{h}+\frac{1}{2}\right)^n + \nu_i \qquad -\frac{h}{2} \le z \le \frac{h}{2} \\ \alpha_T(z) &= (\alpha_{To} - \alpha_{Ti})\left(\frac{z}{h}+\frac{1}{2}\right)^n + \alpha_{Ti} \qquad -\frac{h}{2} \le z \le \frac{h}{2} \\ \beta(z) &= (\beta_o - \beta_i)\left(\frac{z}{h}+\frac{1}{2}\right)^n + \beta_i \qquad -\frac{h}{2} \le z \le \frac{h}{2} \end{aligned} \tag{46}$$

6. Numerical analysis

Numerical outcomes are acquired on the basis of SAPM semi-analytical solution technique which its reliability and validity were confirmed before. Not only for two-dimensional geometries but also for three-dimensional coordinates, the SAPM worked well as a general solution method. Here, in order to avoid any repetition, the SAPM procedure is not re-introduced and it can be simply found in [34-36].

6.1. Validation

First, it is essential to examine whether the obtained results of the governing equations are reliable or not. According to Table 1, the results are presented for a typical cylindrical structure and ABAQUS software. The specifications of the cylindrical structure under consideration are as follows:

$$E = 1900\text{Gpa}; \nu = 0.29; h = 0.01\text{m}; \dot{\theta} = 3\text{rpm}; R = 1\text{m}; L = 5\text{m}$$

The results are presented for two parameters of maximum deformation as well as von Mises stresses for different loads. As explained earlier, the results of the cylindrical structure can be obtained from the torus structure. According to the analyzed cylinder specifications, the torus radius (R_t) is assumed to be infinitely (physically infinite, here $R_t = 10000\,m$ is considered). Therefore, the angle $\alpha = \frac{5}{10000}\ (Rad)$ will be obtained and the radius of the cylinder will be the same as $R = 1\ m$. In Table 1, the evaluation can be considered for both the cylindrical and torus-shape structure. It can be seen that the results of two cylindrical and simulated cylinder based on torus geometry are very similar, and the difference between the two evaluations is not much different from the results obtained from ABAQUS software. Therefore, it can be concluded that the governing equations and the applied solution method are efficient and the results of present analysis can be used with high confidence in further investigations. It is observed that as the internal pressure of the structure increases, the

deformation and the stress increase. For the loading value of q_z = 0.4 *MPa*, the von Mises stress will be around the yield stress of about 206 *MPa*, and for more loads than that, no elastic analysis will prevail and the structure will enter into the plastic deformation zone, which is not desirable. Therefore, the allowable internal pressure limit for the analyzed structure (in these conditions) will be maximum q_z = 0.4 *MPa*.

Table 1. Comparison of present paper (PP) results and ABAQUS for different amounts of loading values

q_z (MPa)	PP		PP		ABAQUS	
	w (mm)		σ_{von} (MPa)		*w* (mm)	σ_{von} (MPa)
	Torus	Cylinder	Torus	Cylinder		
0.1	24.39	24.27	51.83	51.67	24.30	51.72
1	243.9	242.8	518.3	516.7	243.0	517.2
10	2439	2427	5183	5167	2430	5172

6.2. Investigation of important parameters

A cylindrical chamber with radius, thickness and length of *R* = 100 *m*, *h* = 0.1 *m* and *z* = 1000 *m* is considered. The structure rotates around the central axis at a speed of 3 revolutions per minute (RPM). The material properties are the same as in Table 1. The internal pressure of structure is 10^5 Pa (equal to the pressure on the equator). It is worth to be noted that the internal pressure imposed on the analyzed structure's surface is the same as the pressure applied on the sea level, which is about 100 kilo Pascal (*kPa*). The effect of environmental conditions (temperature and humidity changes) is not considered for this special problem. The main question is what the appropriate thickness should be considered in order to be able to withstand the imported loads. On the other hand, could the structure (with the assumed thickness) tolerate the imposed situations successfully or not.

Figures 5a and 5b show the changes in the maximum deformation as well as the von Mises stress occurred in the cylindrical structure versus the length of structure (here is represented by *z*). The main goal here is to have a minimum possible thickness so that the resulted stress in the structure is less than the yield stress of the material (which is about 206 *MPa*). According to Figures 5a and 5b, it can be concluded that the structure can overcome the imposed internal pressure (in absence of environmental conditions) with an acceptable factor of safety. The performed analysis is completely non-linear dynamics [39] and the obtained results are reliable according to the comparison and evaluation that had been made in Table 1.

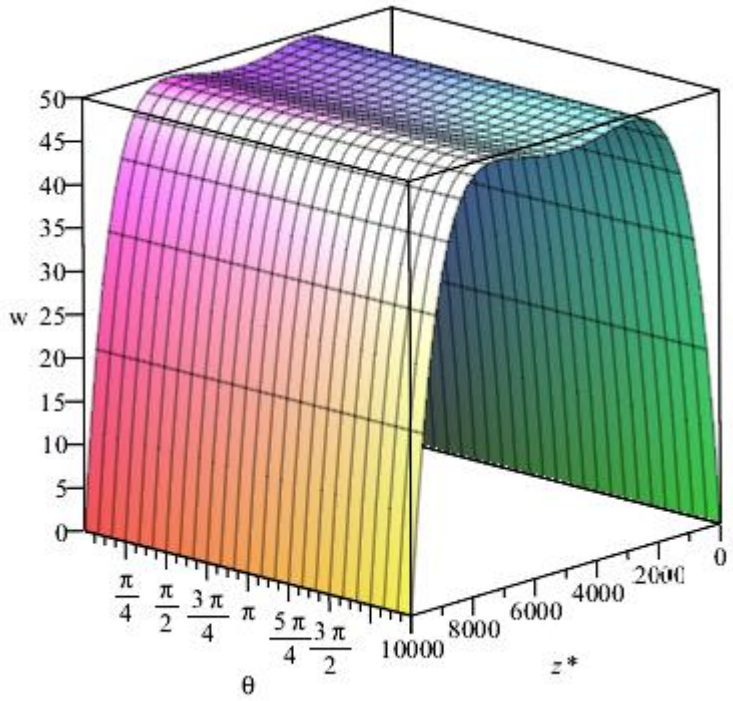

(a)

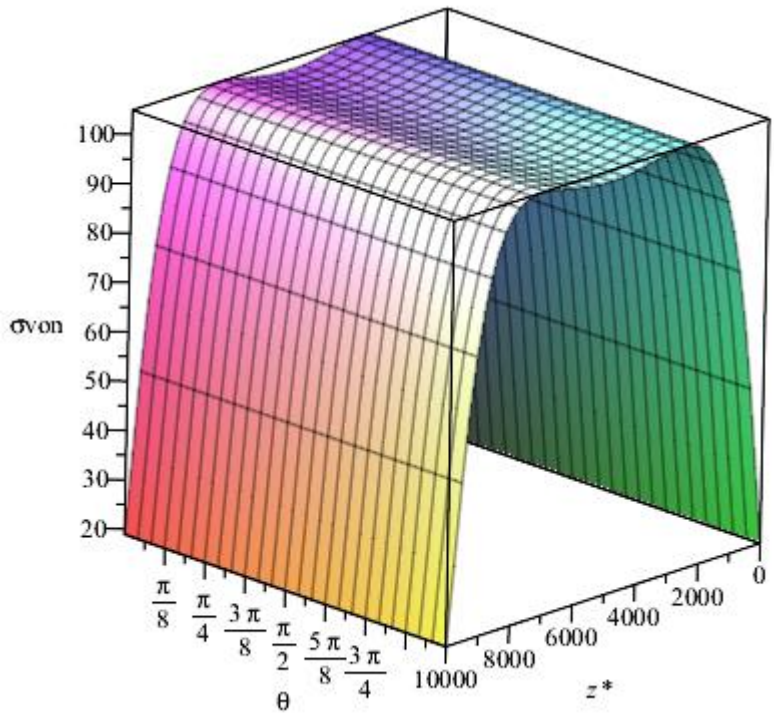

(b)

Fig. 5. Analysis of a cylindrical structure versus θ and $z^* = z/h$ directions for (a) deflection (w) and (b) von Mises (σ_{von}) numerical results

Both of the cylindrical and torus structures are analyzed in this study. The considerations for the temperature of the structure and its effects on the strength of the structures must also be considered. In Figures 6a, 6b, 7a, and 7b, the deflection and von Mises stress changes in the body of the cylindrical structure and torus have been investigated for two temperature differences of 0 and 30℃ against the thickness changes. In all values, the thickness of the structure is observed. For each temperature difference, the deformation and the stress created in the structure increase. Figure 6a shows that if the thickness of the structure is low, temperature changes do not have much effect on the results. But as the thickness increases, the effects of temperature differences on the results become apparent. The slope of changes is initially very steep and descending. However, it is gradually reduced and it can be seen that increasing the thickness of the structure has no effect on reducing the deformation and stresses

in the structure. The mentioned result is more obvious in the case of considering the temperature difference. Deformation and thermal stresses will have a subtle change with the increase of the thickness. Therefore, the greater thickness of the structure will increase significantly the weight of the structure and its production cost. The stresses existed in the structure must be less than the allowable limit so that the structure does not undergo plastic deformation. Creating permanent deformations in structures has many adverse effects that must be avoided. The internal pressure of the structure is due to the followings applied pressures:

1) The simulated internal pressure is equal to 100 *kPa*.
2) The pressure exerted by objects inside the structure on its wall due to their gravitational force.

According to Figure 7a, for the thickness of the structure below 0.1 *m* (h < 0.1 *m*), the stresses raised in the structure will be within the allowable yield limit, which is equal to 206 *MPa*. Therefore, the thickness of the structure should be thicker than 0.1 *m* due to the standard allowable yield stress limit. The difference between the results of the von Mises stresses for the temperature change from 0 to 30℃ is not great, but this difference is about twice that of the deformation results. For example, the difference in deformation results per h = 0.1 *m* in the case of a temperature difference of 0 and 30℃ is about 100%, which is only about 20% in the case of von Mises stresses. According to Figures 6a and 7a for the cylindrical structure, it can be concluded that choosing the thickness of the structure equal to *h* = 0.1 *m* can be appropriate. If the geometry of the studied structure is torus shape, its surface area will be reduced. It is not possible to say exactly which structure is more suitable for creating best conditions. In other words, a cylindrical structure is more appropriate or a torus-shaped structure. Choosing each of them has its own advantages and disadvantages. In Figures 6b and 7b, the obtained results for the cylindrical structure are repeated here for the torus structure. It can be seen that temperature

changes do not play a significant role here, as previously discussed in the cylindrical structure. The results are slightly different for temperatures between 0 and 30℃. But the slope of the changes here is steeper (Figures 6b and 7b). With increasing thickness, the resulted deformation and stress demonstrate a sharp decline. Because here the structure will be very thick.

In the case of a large construction, choosing a cylindrical shape would seem more reasonable. Due to the fact that the deformation in the torus structure is asymmetric and the stress and deformation created in the direction of the θ angle (Fig. 3) are asymmetric, so the uniformity that had been seen in the cylindrical structure no longer exists in the case of the torus structure. Due to the curvature in α and θ directions, the construction of such a donut-shaped complex also has its own challenges, which are expected to be costlier compared to the cylindrical structures. Of course, another advantage of torus-shaped structures is the ability to rotate on two independent axes, α and θ. The only thing that could be done about cylindrical structures was to make centrifugal force by rotating around θ's angle (Fig. 4). The combined rotation around the θ and α axes in torus structures is assumed. Overall, the obtained results from Figures 6 and 7 provide very useful information on the impact of environmental factors such as ambient temperature on the amount of stress and deformation created in cylindrical- and torus-shaped structures. Using the information obtained from Figures 6 and 7, the minimum thickness required for the designed structure can be obtained. Since the equations in this study are general and include many conditions and assumptions, the desired design conditions can be simulated.

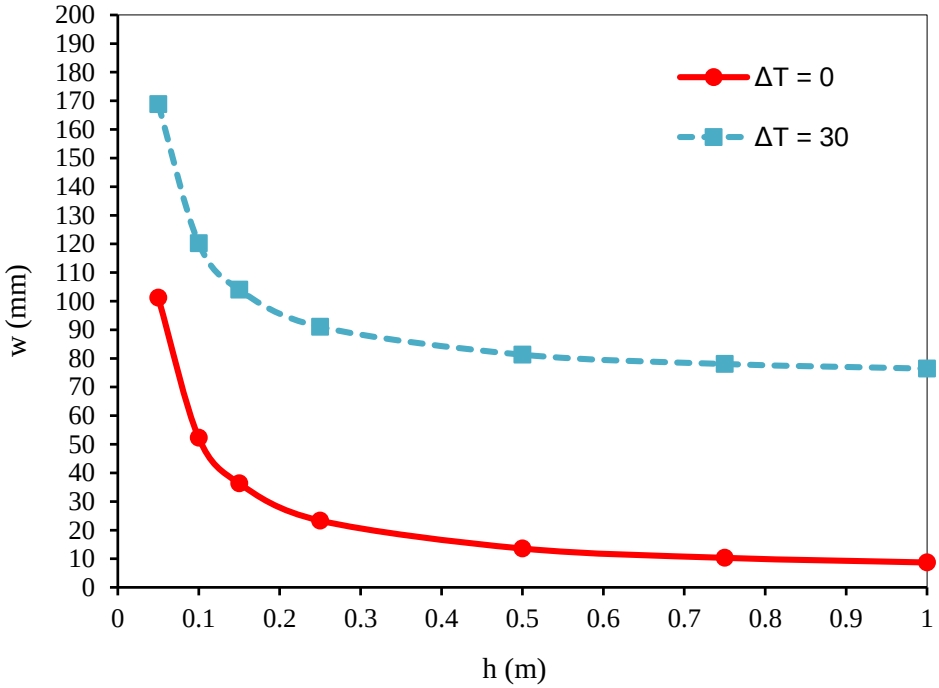

(a)

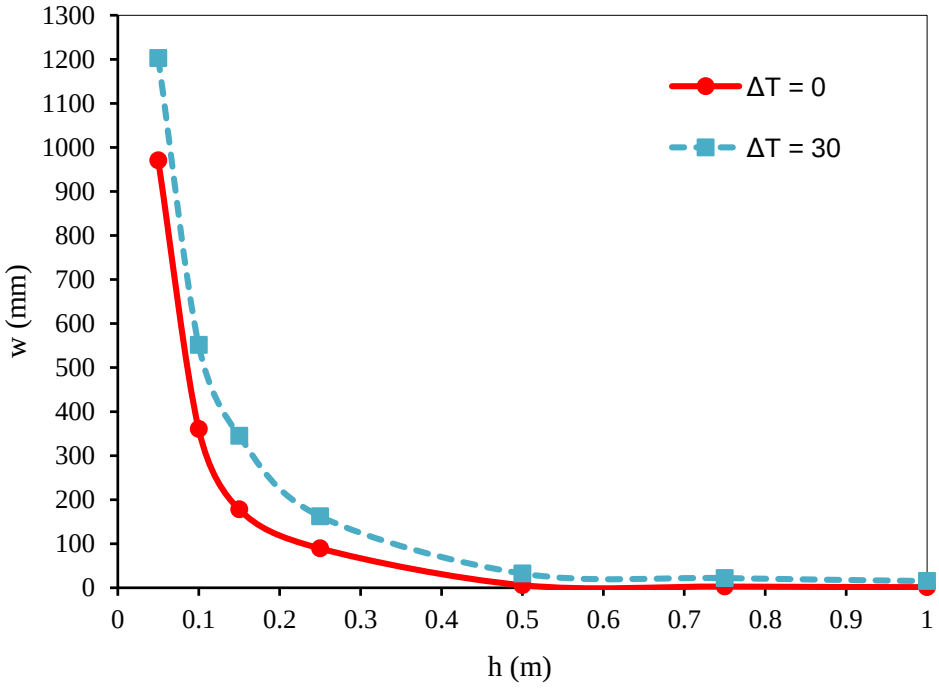

(b)

Fig. 6. Variation of maximum deflection due to increase of thickness (*h*) for different values of □T (a) Cylindrical (b) donut shape structures

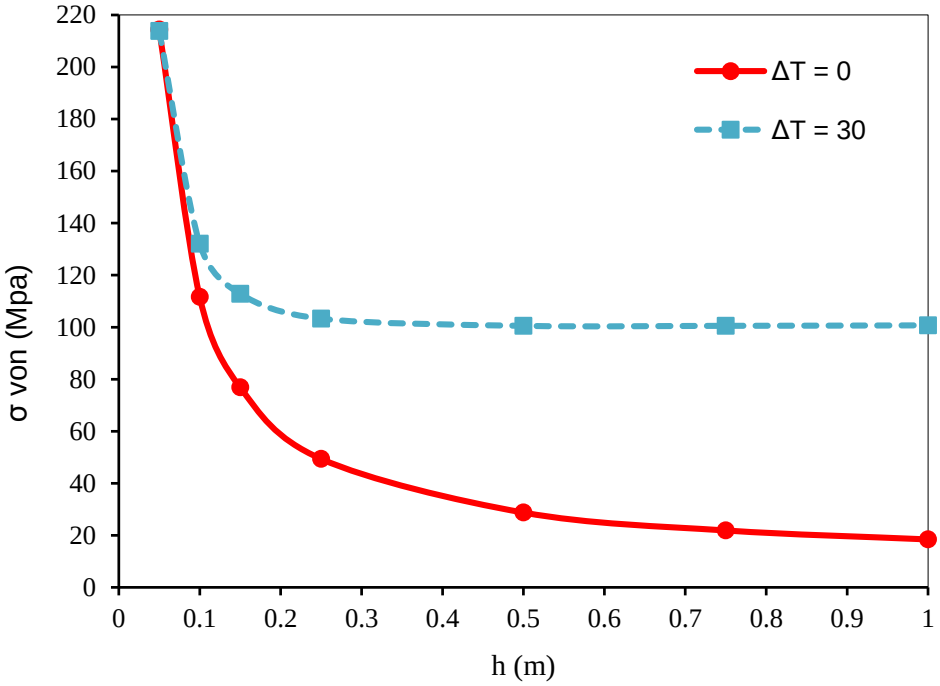

(a)

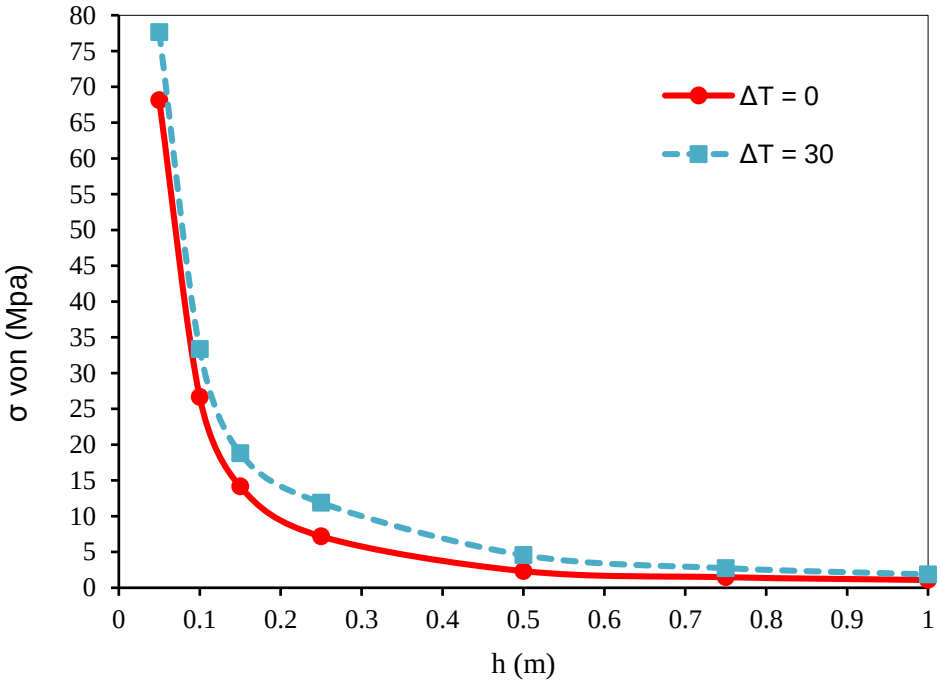

(b)

Fig. 7. Variation of von Mises stress (σ_{von}) due to increase of thickness (h) for different values of □T (a) Cylindrical (b) donut shape structures

In Figures 6a, 6b, 7a and 7b, the effect of temperature changes on the results of deformation and stress in the structure was investigated. Another environmental factor that affects the results is the humidity of the environment, which affects the deformation and stresses created in the body of the structure. Standard humidity should be considered in the life environment of the structures in order to facilitate and normalize conditions. Figures 8 and 9 show the effect of ambient moisture content (□H) on the obtained results. The results are plotted for two values of temperature difference (□T). It is observed that the maximum deformation of the structure for two values of temperature difference of □T = 0 and 30℃ show almost the same behavior (the slope of the changes is almost the same with a slight difference). As □H increases, the deformation of the structure increases as well, but this increase is not very significant and can be ignored in comparison with the changes caused by temperature. In other words, in similar conditions, temperature changes affect the structure more than changes in humidity. But here, because research on abnormal conditions is considered, even small and imperceptible changes can be important and should be considered to avoiding very staggering costs that have been incurred. In this research, which has further theoretical aspects, only a few of these factors such as internal pressure, environmental conditions such as temperature and humidity have been mentioned. Therefore, if a practical project is defined for this purpose, a series of factors that are involved in designing a suitable structural system (even factors with a small impact factor) should be considered. Interestingly, according to Fig. 9, if the temperature difference is not taken into account, changes in □H will not affect the stress exerted in the structure and the von Mises stress shows a constant value (Here about 30 MPa). But with increase of the temperature difference (which is closer to the reality of analyzed problem) increase of □H will cause a gradual growth (slightly and with a gentle slope) in von Mises stress.

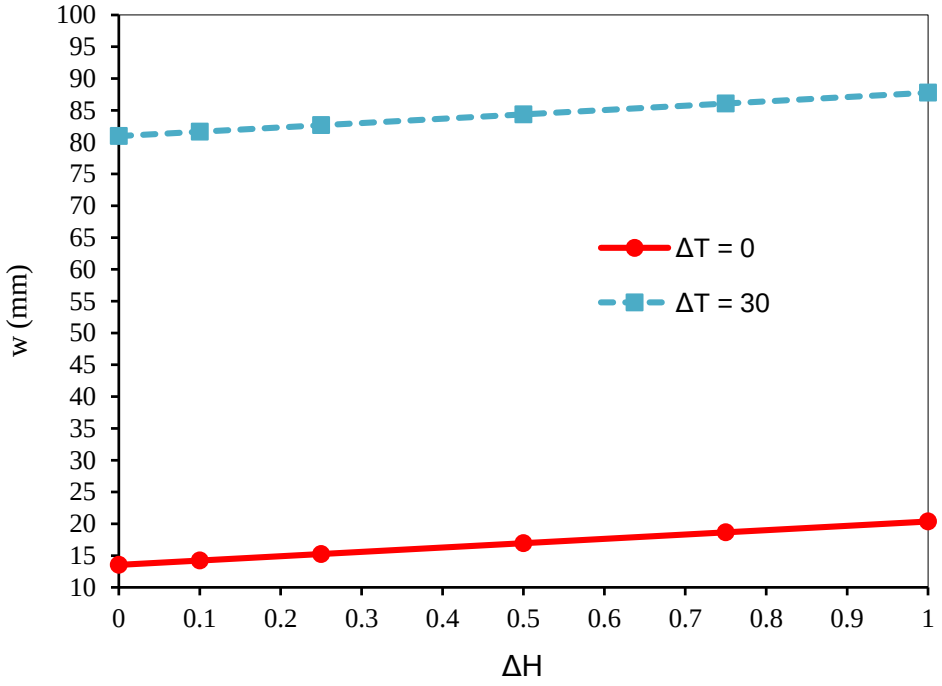

Fig. 8. Variation of the deflection versus the increase of □H for two different values of temperature changes □T = 0, 30℃

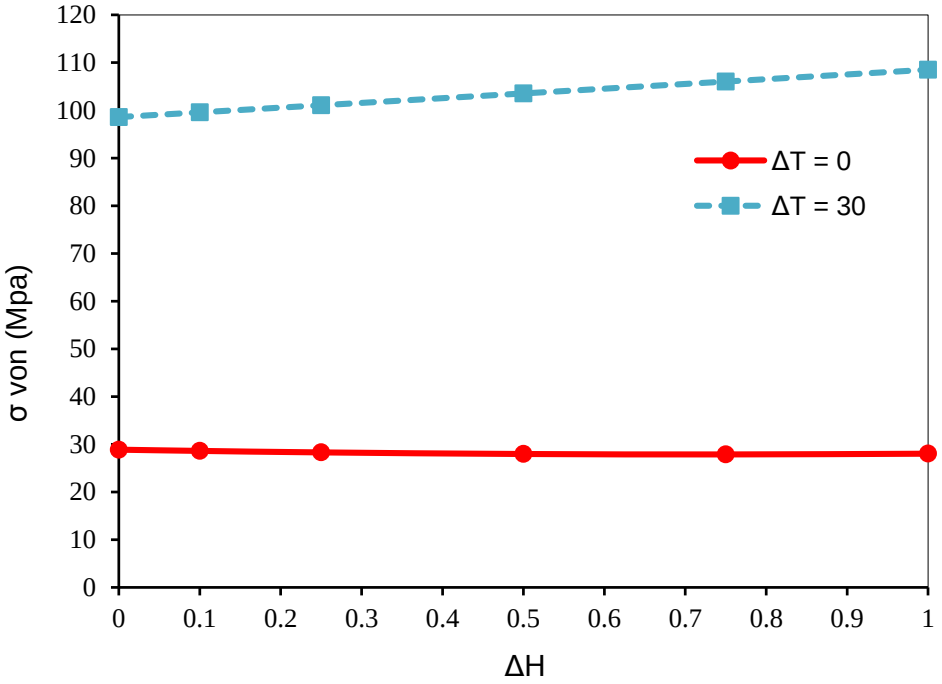

Fig. 9. Variation of von Mises stress results versus the increase of □H for two different values of temperature changes □T = 0, 30℃

One of the most important factors that affects the strength of the structure under analysis is the choice of material. Recently, the use of functionally graded materials (FGM) in which the properties of matter change in one or more directions has been considered by many researchers. This can also be used in the high sensitive industries. Figures 10 and 11 show the maximum deflection and von Mises stresses of a rotating cylindrical structure along the length of the structure for different values of the parameter n (parameter of the intensity of changes from metal to ceramic properties). It is observed that with increasing n, maximum deformation of the structure increases and the resulting von Mises stress decreases. The rate of change in von Mises stress is more severe than the deformation rate. By increasing parameter n, initially the changes in Figures 10 and 11 are large, and in continue with increasing n, no noticeable changes are observed. According to Figures 10 and 11, it can be concluded that the selection of FGM materials reduces the stress of the structure, so it is possible to use functional materials in the analyzed structure to aim acquiring the desired thickness followed by a decrease (appropriate thickness according to Figures 6 and 7). Here, if the parameter n is selected, for example equal to 5, about 60% of the stress created in the structure will be reduced, while only about 20% will be added to the deformation of the structure. Therefore, it can be possible to use FGM material with the mentioned specifications and parameter $n = 5$. But using FGM materials costs a lot. However, with the development of their manufacturing technology so that their production costs are significantly reduced (due to their unique characteristics), and it will be widely used in high sensitive structures. It should be noted that the values of the horizontal axis in Figures 10 and 11 are dimensionless ($z^* = z/h$). The order of use of FGM materials in conditions where the influence of environmental factors such as humidity and temperature variations is considered, can optimize the design of the structure and significantly increase its strength.

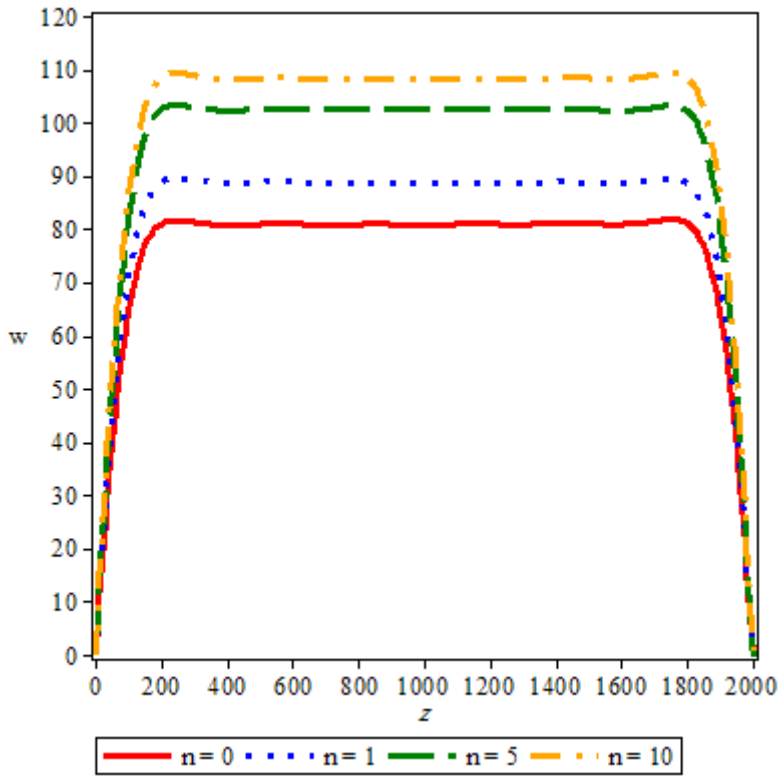

Fig. 10. Deflection changes (in millimeter) along the length of structure (in meter) for different values of parameter *n*

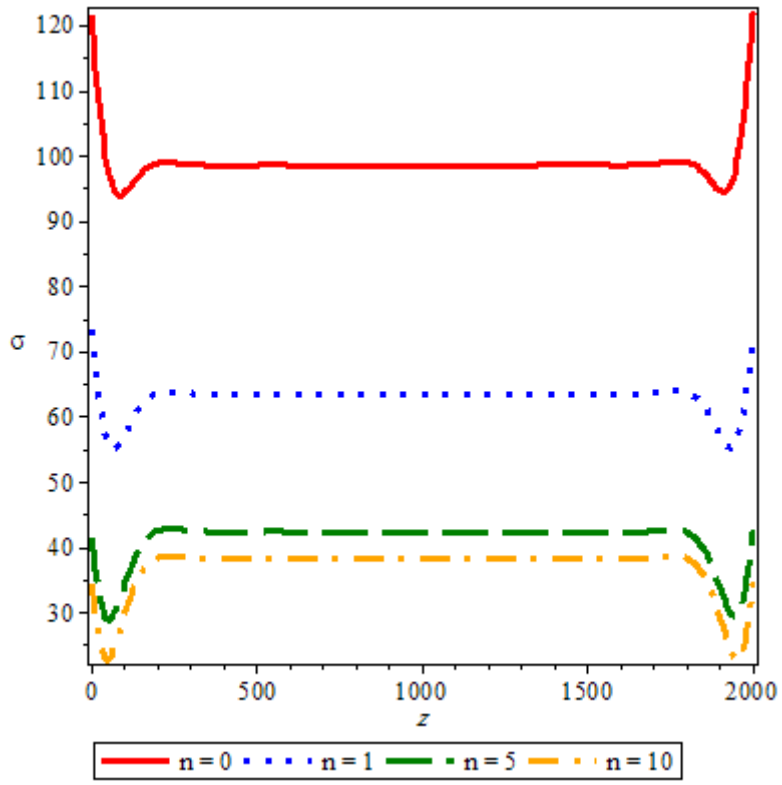

Fig. 11. Von Mises stress changes (in MPa) along the length of structure (in meter) for different values of parameter *n*

The rotating motion around a center should not cause inconvenience to the inhabitants of the structure. The tolerance of machine at different rotational speeds is a criterion that should be considered in the design of structure. If the rotational speed around the central axis is accelerated, this will also cause problems. Therefore, accelerated rotational speed should be avoided. In other words, in the obtained governing equations of the cylindrical structure $\dot{\theta} = 0$ should be considered, and in the torus structure $\dot{\alpha} = \dot{\theta} = 0$.

Figures 12 and 13 show the effect of rotational speed on the strength of the cylindrical structure. Fig. 12 examines the changes in the maximum deformation of the structure and Fig. 13 examines the von Mises stresses occurred in the structure in exchange for increasing the rotational velocity in both states (a) and (b). Details of modes (a) and (b) are as follows:

(a) □T = 30℃, □H = 0.2

(b) □T = 0, □H = 0

As can be seen, the resulting deformations as well as the von Mises stresses will be greater in condition (a) than in condition (b). However, the difference between the deformation results of conditions (a) and (b) is more obvious. At the beginning of the change, the difference between the two results (conditions (a) and (b)) is greater for the lower rotational velocities, but as the rotational velocity increases, the results of conditions (a) and (b) become closer to each other. For a rotational speed of 10 revolutions per minute (rpm), the results are almost the same. In other words, if the rotational speed of the set has a significant increase, the effects of rotational speed will be greater than other factors such as internal pressure and environmental factors such as temperature and humidity. Consequently, other factors can be ignored compared to rotational speed. In the case of the structure under analysis, the rotational speed is about 3 rpm. But the unwanted rotational speeds happened in the structure up to about 10 rpm will not have much effect on the structure and for example the von Mises stress is about 150 MPa (when the rotational speed is 10 rpm) and in rotational speeds lower in the range of 0 to 10 rpm, the stress is about 100 MPa. But by doubling the rotational speed from 10 to 20 rpm, the von Mises stress in the structure will be about 460 MPa at once, which is about three times greater than the stress when the rotational speed is 10 rpm. This created stress is more than twice the allowable yield stress of the selected material and if the structure rotates at this rotational speed, the disintegration of the structure is not far from the mind. However, the more important issue to consider is the destructive effect of such a rotational speed for the connected parts.

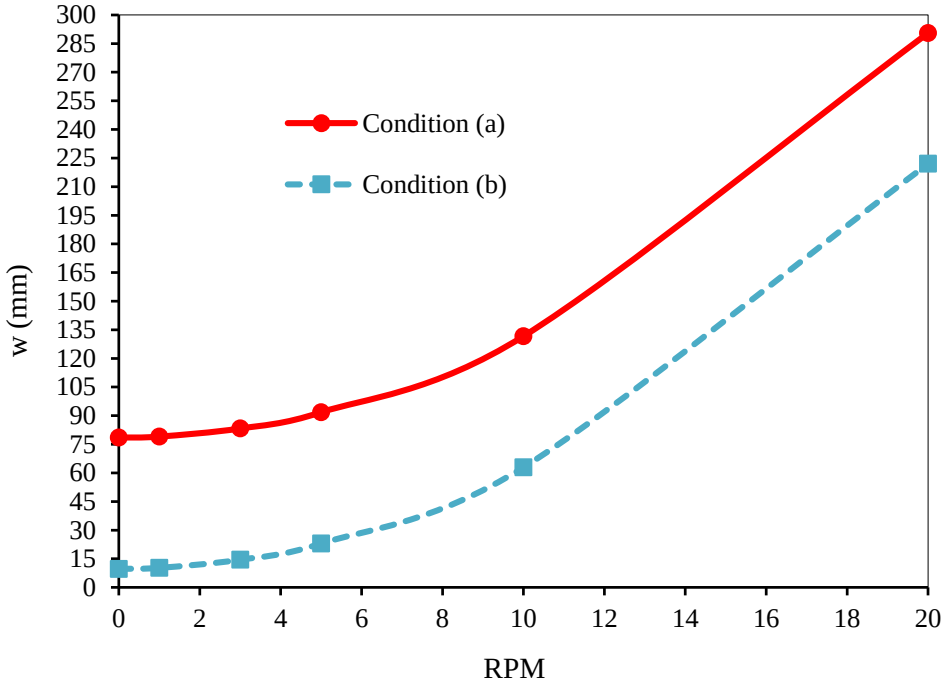

Fig. 12. Deflection changes versus the rotation velocity of structure for two types of conditions (a) and (b)

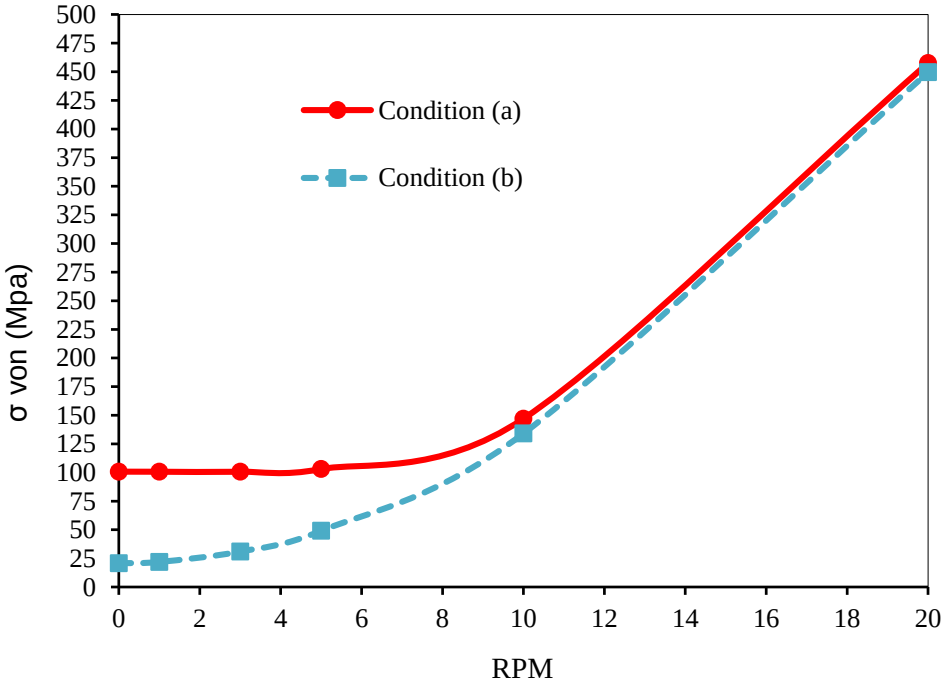

Fig. 13. Von Mises stress changes versus the rotation velocity of structure for two types of conditions (a) and (b)

The selection of the appropriate thickness for the structure that was examined in Figures 6 and 7 should now be studied more closely. For example, if the thickness of the structure is considered to be 20 *cm*, choosing this thickness throughout the structure will cause a huge increase in the mass of the complex and its staggering costs. In practice, structures are composed of a thin layer of coating, most of which is responsible for preventing the penetration of vital gases such as oxygen, heat and moisture storage inside the structure, which is vital for the life of internal parts and protection against harmful conditions. Also, a skeleton holding the internal equipment and supporting the outer cover, which is responsible for withstanding the mechanical and environmental loads on it, has been formed. In practice, for a section of housing structure, the thickness (that is uniformly distributed) can be simulated with a truss structure, in which the loads, stress and deformation created in the structure are equivalent. Fig. 14 shows this equivalence schematically.

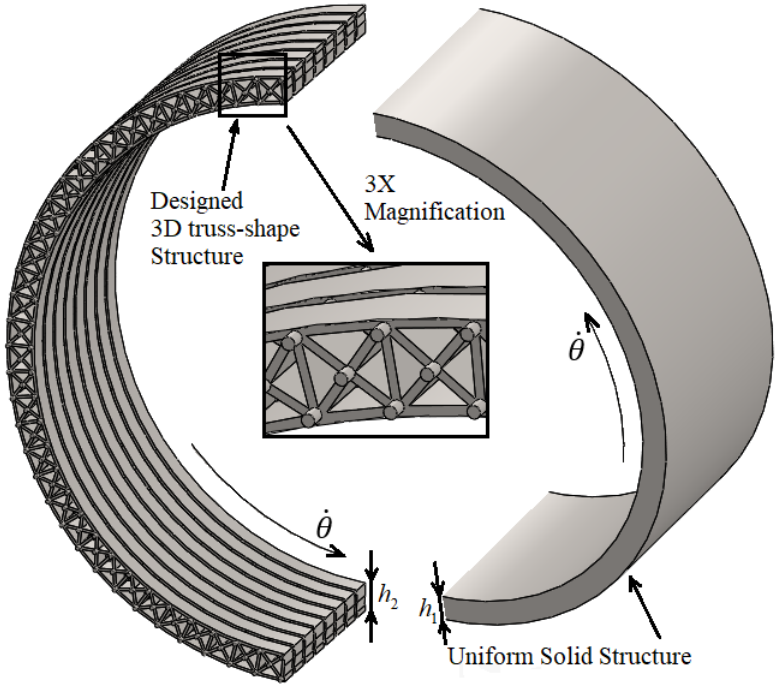

Fig. 14. Schematic view of designed hollow structure versus its equivalent uniform solid structure

The equivalence state specified in Fig. 14 can be assumed in such a way that the structure with uniform and integrated thickness has a defective porosity [40, 41]. The mechanical response should be equal for a uniform structure (right in Fig. 14 with thickness h_1) and the same porous structure (left in Fig. 14 with thickness h_2). By obtaining the equivalent thickness to the section with structural defect, the thickness of the designed structure can be calculated equal to the obtained thickness of the section with porosity defect. This issue has been studied in this research for the first time from a mechanical point of view and needs further study and research. Equating structures with and without structural porosity defects can significantly reduce the simulation time and costs. From a theoretical point of view, as the thickness of a structure increases, the deformations and stresses created in the model will decrease, and from a mechanical point of view, the reliability of the structure against the applied loads increases. Nevertheless, this will increase the mass, in consequence, increase the cost of construction and in this particular case will make it impossible to carry out the project (because the environmental conditions are abnormal and pose many challenges).

The structural defect of porosity is defined by a factor (□). In other words, the higher the □ value, which indicates a structural defect, the lower the strength of the material. The structural defect of porosity in both even and uneven modes can have an effect on the Young's elasticity modulus of the material, like the following equations.

Even Porosity: $$E(z)=(E_o-E_i)\left(\frac{1}{2}+\frac{z}{h}\right)^n+E_i-\frac{\lambda}{2}(E_o+E_i) \quad (47)$$

Uneven Porosity: $$E(z)=(E_o-E_i)\left(\frac{1}{2}+\frac{z}{h}\right)^n+E_i-\frac{\lambda}{2}(E_o+E_i)\left(1-\frac{2|z|}{h}\right) \quad (48)$$

Fig. 15 shows the maximum deflection variations of a rotating cylindrical structure versus an increase of the thickness of the structure for different □coefficient values. □= 0 indicates

a state in which there is no defect in the structure and the material distribution is considered integrated. It is observed that with the increase of □ coefficient, the deformations created in the structure increase. As the amount of □ increases, the effect of its increase on the results becomes more apparent. In other words, it can be said that a 25% increase in the □ coefficient in a structure that already has about 25% structural defects, compared to the case where the structure is without defects (□ = 0) and its structural defect increases to 25%, it will present more deformation in the structure. It can be assumed that in the case of a structure with a structural defect of 50%, half of the internal space of the structure is filled with empty spaces. According to Fig. 15, for example, for deformations equal to about 80 *mm* for a flawless structure and a structure with a defect of 30%, the thickness of the non-defected structure is approximately 0.7 *m* and the thickness of the defected structure should be equal to 1.5 *m* (almost more than twice as much). It should be noted that for a 50% defected structure, this thickness must be equal to 2.5 *m*. Even the thickness of the structure without defect in this case will be equal to 0.6 *m*. That is, a 50% increase in the structure defect requires a thickness equal to about 4 times the thickness of the defected structure so that the deformations created in it (50% defected structure) are equal to the deformations of a defected structure. A thickness of 2.5 *m* with a structural defect of 50% represents about half of the empty space inside the structure that a network can be considered in this case. For example, this defected thickness can be simulated with a 3D truss and the skeleton design of the structure could be considered based on its ability to withstand the applied loads. The cross section of a 3D truss sample designed in this study (using the obtained results from the thickness equated to a flawless structure with a structural defect of 50%) can be seen in Fig. 14.

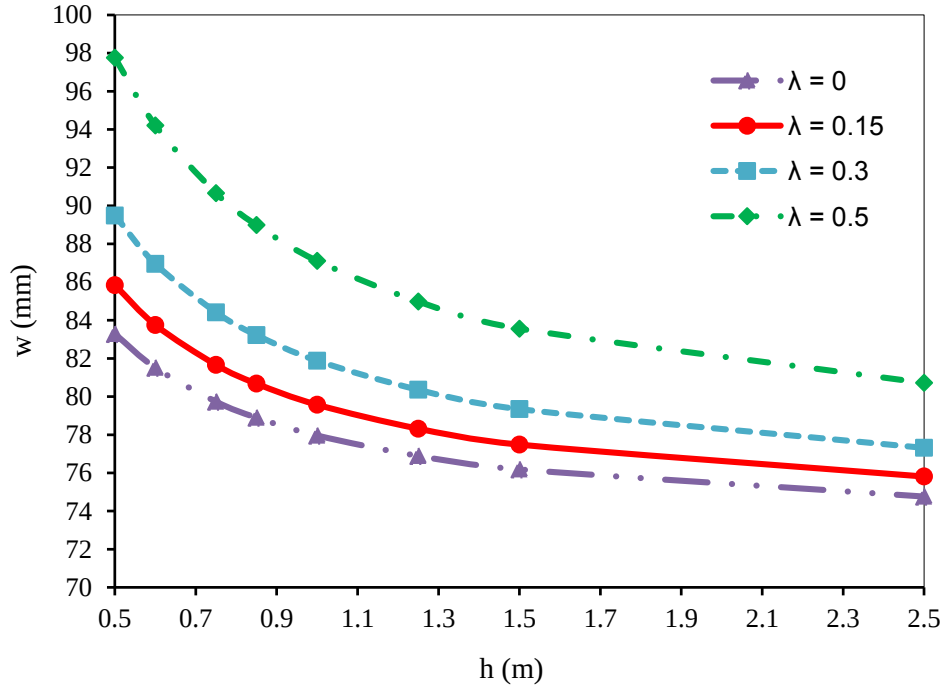

Fig. 15. The effect of porosity (even) on the deflection results of rotating structure versus the thickness of structure for different values of porosity factor □

Fig. 15 demonstrated the effect of structural defect factor on the deflection results. It also takes into account the environmental effects of temperature and humidity. Nevertheless, if the environmental effects are ignored, for a structure to have a porous defect equal to 50%, the maximum deflection can be plotted in terms of thickness increase, in which the results are shown in Fig. 16. It is observed in this case, the effect of the structural defect on the results is much greater. According to Fig. 15, for □= 0.5, deflection experiences a 20% reduction from 100 *mm* to 80 *mm*. Conclusion that has previously obtained (Fig. 15) in which the environmental factors of temperature and humidity were omitted, there was a reduction of approximately 60% (from 29 to 12 *mm*).

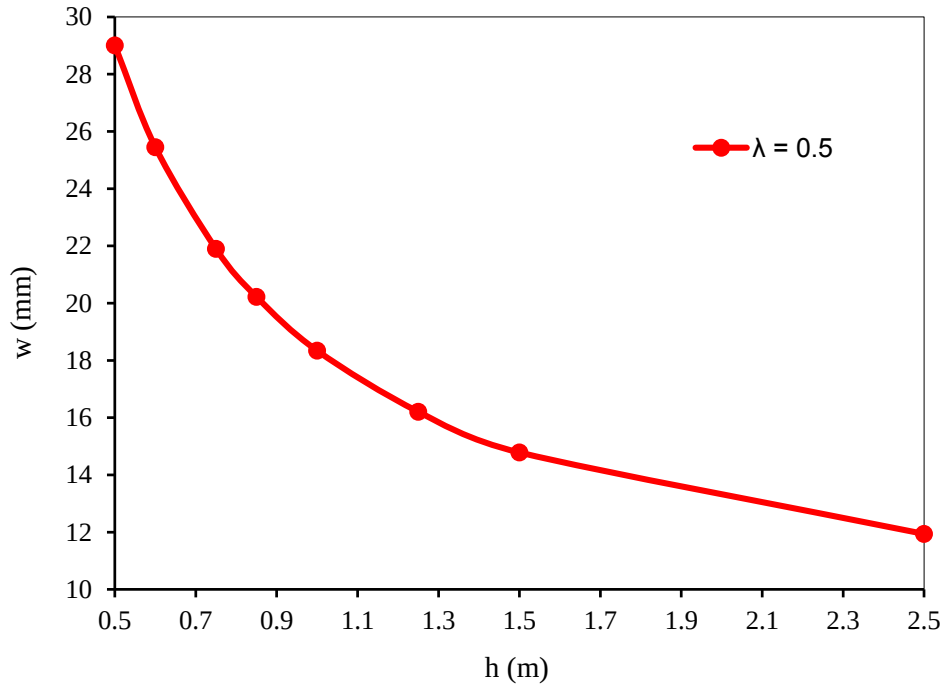

Fig. 16. Deflection changes of rotating structure versus the thickness of structure for □ = 0.5 and □T = □H = 0

Comparing Fig. 15 and 16 shows that environmental factors play a very important role in the design of high-sensitive structures, and ignoring them can cause serious errors in calculations. Therefore, even the smallest details should be considered in the simulation and design of these structures. This study is used as a theoretical example in simulating rotating structures for the best wind energy harvester and similar to the normal conditions. The further analysis can involve more details, such as magnetic fields [42], viscoelastic modelling of wind turbine parts [43] and various external forces.

7. Conclusions and remarks

In this study, the mechanical strength of cylindrical and torus structures against internal pressures and environmental factors (temperature and humidity) was investigated. The mechanical modeling is presented based on a general first-order shear deformation shell theory. The calculated formulas are in a general form in which many other theories could be applied.

Centrifugal forces within the structure is simulated due to the rotation of the structure around the central axes. The obtained equations are completely non-linear dynamic and include the effects of rotation of the structure on the resulted deformation and stresses. The factors affecting the problem are presented and interpreted in the form of numerical analysis (graphs). In general, the most important results can be summarized and categorized as follows:

- Simulation of centrifugal forces and its effects on the strength of cylindrical- and torus-shaped structures are different, and the choice of each structure has its own advantages and disadvantages. In general, the torus-shaped structure has more resistance than the cylindrical structure.
- Considering the environment conditions outside the structure, the environmental factors such as pressure, temperature and humidity will have a great impact on the strength of the structure and their effects should be considered in the calculations.
- The use of FGM materials in high-sensitive structures greatly increases its strength. Therefore, with less thickness and the use of FGM materials, the desired strength can be taken in the applied structure.
- By using the method presented in this research, it is possible to calculate the equivalent thickness to design the shape of the analyzed structure (here a three-dimensional truss).
- The rotation of the structure (which causes centrifugal forces) has a negative effect on its strength. If the rotation of the structure is more than expected, it will cause its destruction.

Acknowledgments: V.A.E. acknowledges the support by grant 14.Z50.31.0036 awarded to R. E. Alekseev Nizhny Novgorod Technical University by Department of Education and Science of the Russian Federation.

References

[1] V. N. Skopinsky, Stress analysis of shell intersections with torus transition under internal pressure loading, ASME, 119 (1997) 288-292.

[2] F. Li, H. Chen, K. Mao, Computational simulation analysis for torus radius of edge contact in hip prostheses, Acta of Bioengineering and Biomechanics, 17 (2015) 67-73. DOI: 10.5277/ABB-00149-2014-04

[3] A. Rajan, J. Kochupillai, Dynamic analysis of a pressure prestressed in vacuo torus with follower load stiffness, Proc IMechE Part C: Journal of Mechanical Engineering Science, 229 (2015) 1760–1768.

[4] D. Overbeye, New York Times 11 March 2003: Web. 16 January 2011.

[5] J. Levin, E. Scannapieco, J. Silk, The topology of the universe: the biggest manifold of them all, Classical and Quantum Gravity, 15 (1998) 2689.

[6] M. J. Muliawan, M. Karimirad, T. Moan, Z. Gao, STC (Spar-Torus Combination): A Combined Spar-Type Floating Wind Turbine and Large Point Absorber Floating Wave Energy Converter — Promising and Challenging, Proceedings of the ASME 2012 31st International Conference on Ocean, Offshore and Arctic Engineering. Volume 7: Ocean Space Utilization; Ocean Renewable Energy. (2012) 667-676. https://doi.org/10.1115/OMAE2012-84272

[7] Z. Gao, T. Moan, L. Wan, C. Michailides, Comparative numerical and experimental study of two combined wind and wave energy concepts, Journal of Ocean Engineering and Science, 1 (2016) 36-51.

[8] N. Ren, Z. Gao, T. Moan, L. Wan, Long-term performance estimation of the Spar–Torus-Combination (STC) system with different survival modes, Ocean Engineering, 108 (2015) 716-728.

[9] A. Clément, P. McCullen, A. Falcão, A. Fiorentino, F. Gardner, K. Hammarlund, G. Lemonis, T. Lewis, K. Nielsen, S. Petroncini, Wave energy in europe: current status and perspectives, Renewable and sustainable energy reviews, 6 (2002) 405–431.

[10] H. Bagbanci, D. Karmakar, C. Soares, Review of offshore floating wind turbines concepts, CRC Press, (2012) 553–562.

[11] M. J. Muliawan, M. Karimirad, T. Moan, Dynamic response and power performance of a combined Spar-type floating wind turbine and coaxial floating wave energy converter, Renewable Energy, 50 (2013) 47-57.

[12] M. J. Muliawan, M. Karimirad, M., Z. Gao, T. Moan, Extreme responses of a combined spar-type floating wind turbine and floating wave energy converter (stc) system with survival modes, Ocean Engineering, 65 (2013) 71 – 82.

[13] L. Wan, Z. Gao, T. Moan, Experimental and numerical study of hydrodynamic responses of a combined wind and wave energy converter concept in survival modes, Coastal Engineering, 104 (2015) 151–169.

[14] Y. B. Bae, M. H. Kim, S. W. Im, Aero-Elastic-Control-Floater-Mooring Coupled Dynamic Analysis of Floating Offshore Wind Turbines, International Society of Offshore and Polar Engineers, (2011).

[15] J. Jonkman, S. Butterfield, W. Musial, G. Scott, De nition of a 5-MW Reference Wind Turbine for Offshore System Development, National Renewable Energy Laboratory, Boulder, 2009 Technical Report NREL/TP-500-38060.

[16] G. Sagli Baarholm, S. Haver, O. D. Okland, Combining contours of significant wave height and peak period with platform response distributions for predicting design response, Marine Structures, 23 (2010) 147-163.

[17] J. M. Choung, Fatigue Design of Mooring Lines of Floating Type Combined Renewable Energy Platforms, International Journal of Ocean System Engineering, 1 (2011) 171-179.

[18] M. I. Kvittem, T. Moan, Time domain analysis procedures for fatigue assessment of a semi-submersible wind turbine, Marine Structures, 40 (2015) 38-59.

[19] M. Karimirad, T. Moan, A simplified method for coupled analysis of floating offshore wind turbines, Marine Structures, 27 (2012) 45-63.

[20] T. J. Larsen, T. D. Hanson, A method to avoid negative damped low frequent tower vibrations for a oating, pitch controlled wind turbine, Journal of Physics, The Science of Making Torque from Wind, IOP Publishing, Conference Series, 75 (2007) 012073, doi:10.1088/1742-6596/75/1/012073, 2007.

[21] J. Zhang, Z. Xiang, Y. Liu, Quasi-Static Shape Control of Flexible Space Structures by Using Heaters, AIAA Journal, 51 (2013) 1003-1007.

[22] W. Yue, Y. Xue, Y. Liu, High Humidity Aerodynamic Effects Study on Offshore Wind Turbine Airfoil/Blade Performance through CFD Analysis, International Journal of Rotating Machinery, (2017). https://doi.org/10.1155/2017/7570519

[23] S. Hassan Danook, K. Joir Jassim, A. Mohammed Hussein, The impact of humidity on performance of wind turbine, Case Studies in Thermal Engineering, 14 (2019) 100456.

[24] A. Kusiak, A. Verma, Analyzing bearing faults in wind turbines: A data-mining approach, Renewable Energy, 48 (2012) 110-116.

[25] J. B. Jorgensen, B. F. Sorensen, C. Kildegaard, The effect of residual stresses on the formation of transverse cracks in adhesive joints for wind turbine blades, International Journal of Solids and Structures, 163 (2019) 139-156.

[26] M. Malikan, V. A. Eremeyev, A new hyperbolic-polynomial higher-order elasticity theory for mechanics of thick FGM beams with imperfection in the material composition, Composite Structures, 249 (2020) 112486.

[27] B. Karami, M. Janghorban, On the mechanics of functionally graded nanoshells, International Journal of Engineering Science, 153 (2020) 103309.

[28] A. M. Dehrouyeh-Semnani, E. Dehdashti, M. R. Hairi Yazdi, M. Nikkhah-Bahrami, Nonlinear thermo-resonant behavior of fluid-conveying FG pipes, International Journal of Engineering Science, 144 (2019) 103141.

[29] M. H. Jalaei, □. Civalek, On dynamic instability of magnetically embedded viscoelastic porous FG nanobeam, International Journal of Engineering Science, 143 (2019) 14-32.

[30] A. Gholipour, M. H. Ghayesh, Nonlinear coupled mechanics of functionally graded nanobeams, International Journal of Engineering Science, 150 (2020) 103221.

[31] R. C. Batra, G. J. Nie, Torsional deformations and material tailoring of orthotropic bi-directional FGM hollow truncated conical cylinders with curved lateral surfaces, International Journal of Engineering Science, 133 (2018) 336-351.

[32] C. Evci, M. Gülgeç, Functionally graded hollow cylinder under pressure and thermal loading: Effect of material parameters on stress and temperature distributions, International Journal of Engineering Science, 123 (2018) 92-108.

[33] B. Karami, D. Shahsavari, M. Janghorban, L. Li, On the resonance of functionally graded nanoplates using bi-Helmholtz nonlocal strain gradient theory, International Journal of Engineering Science, 144 (2019) 103143.

[34] Sh. Dastjerdi, B. Akgöz, New static and dynamic analyses of macro and nano FGM plates using exact three-dimensional elasticity in thermal environment, Composite Structures, 192 (2018) 626-641.

[35] Sh. Dastjerdi, B. Akgöz, On the statics of fullerene structures, International Journal of Engineering Science, 142 (2019) 125-144.

[36] Sh. Dastjerdi, B. Akgöz, Ö. Civalek, On the effect of viscoelasticity on behavior of gyroscopes, International Journal of Engineering Science, 149 (2020) 103236.

[37] V. A. Eremeyev, G. Rosi, S. Naili, Transverse surface waves on a cylindrical surface with coating, International Journal of Engineering Science, 147 (2020) 103188.

[38] A. Eyvazian, D. Shahsavari, B. Karami, On the dynamic of graphene reinforced nanocomposite cylindrical shells subjected to a moving harmonic load, International Journal of Engineering Science, 154 (2020) 103339.

[39] A. A. Gholampour, M. Ghassemieh, J. Kiani, State of the art in nonlinear dynamic analysis of smart structures with SMA members, International Journal of Engineering Science, 75 (2014) 108-117.

[40] Q. Zhang, H. Liu, On the dynamic response of porous functionally graded microbeam under moving load, International Journal of Engineering Science, 153 (2020) 103317.

[41] B. Karami, D. Shahsavari, M. Janghorban, On the dynamics of porous doubly-curved nanoshells, International Journal of Engineering Science, 143 (2019) 39-55.

[42] M. Malikan, M. Krasheninnikov, V. A. Eremeyev, Torsional stability capacity of a nano-composite shell based on a nonlocal strain gradient shell model under a three-dimensional magnetic field, International Journal of Engineering Science, 148 (2020) 103210.

[43] P. J. Hine, A. A. Gusev, Validating a micromechanical modelling scheme for predicting the five independent viscoelastic constants of unidirectional carbon fibre composites, International Journal of Engineering Science, 144 (2019) 103133.